INSTITUTO POLITÉCNICO DE LISBOA

ESCOLA SUPERIOR DE TECNOLOGIA DA SAÚDE DE LISBOA

DOSIMETRIC CRITERIA FOR PLAN ADAPTATION IN CHARGED PARTICLE THERAPY FOR PANCREATIC TUMOUR PATIENT

COMPOSED BY ZANEERA ASIM

AT THE UNIVERSITY CLINIC OF HEIDELBERG, GERMANY

SUPERVISED BY VÂNIA BATISTA

CO-SUPERVISED BY PROF. PAULO FERREIRA

MASTERS IN RADIATIONS APPLIED TO HEALTH TECHNOLOGIES

\- RADIATION THERAPY -

LISBON, OCTOBER 2016

INSTITUTO POLITÉCNICO DE LISBOA

ESCOLA SUPERIOR DE TECNOLOGIA DA SAÚDE DE LISBOA

DOSIMETRIC CRITERIA FOR PLAN ADAPTATION IN CHARGED PARTICLE THERAPY FOR PANCREATIC TUMOUR PATIENT

COMPOSED BY ZANEERA ASIM

AT THE UNIVERSITY CLINIC OF HEIDELBERG, GERMANY

SUPERVISED BY VÂNIA BATISTA

CO-SUPERVISED BY PROF. PAULO FERREIRA

JURY:

DR. MARGARIDA EIRAS - ESCOLA SUPERIOR DE TECNOLOGIA DA SAÚDE DE LISBOA (PRESIDENT)

DR. NUNO TEIXEIRA - ESCOLA SUPERIOR DE TECNOLOGIA DA SAÚDE DE LISBOA (ARGUER)

VÂNIA BATISTA - UNIVERSITY CLINIC OF HEIDELBERG (SUPERVISOR)

MASTERS IN RADIATIONS APPLIED TO HEALTH TECHNOLOGIES

- RADIATION THERAPY -

LISBON, OCTOBER 2016

Declaration

I, Zaneera Asim, declare that this thesis, submitted in the fulfillment of the Master's degree at Escola Superior de Tecnologia da Saúde de Lisboa, is wholly my own work unless otherwise referenced or acknowledged appropriately.

Zaneera Asim

October 2016

Acknowledgment

Firstly, I would like to acknowledge my thesis supervisors and thank them for their support. I am extremely thankful to Vânia Batista for being such a wonderful mentor over the past few months. Her friendly guidance, support in every aspect and almost 24/7 availability made me capable to complete this thesis. She has been a great source of encouragement to me and greatly enhanced my understanding of the work. This experience gave me an unattainable insight into the clinical aspects of charged particle therapy and was truly a wonderful time. I also appreciate the support from Prof. Paulo Ferreira for not only supervising me along the thesis but his contribution throughout the masters program. Thanks also to Dr. Oliver Jäkel for his support in the enhancement of my knowledge.

Thanks to those who were involved in SPARTA project and supported in this thesis, especially Wenjing Chen and Julia Bauer. I would like to thank Dr. Patrick Naumann for his support in delineating the OARs. I appreciate Dr. Naved Chaudhry and Asiya Khan for sparing time to review my thesis. I would like to thank Prof. Margarida Eiras and Prof. Ana Vasconcelos for their guidance in selecting a thesis topic and making this process easier for me.

I would also like to express my appreciation to the fellows at Heidelberg Ion-Beam Therapy for making my time memorable in Heidelberg despite being far from home.

Finally, thanks to my family.

Abstract

Charged particle beam therapy has been used for its twofold advantageous behavior: offering high precision to the target volume and minimum doses to organs at risk and normal function tissue. Treatment outcome of pancreatic patients is compromised by dose limits of the gastrointestinal tract and dose escalation is critical due to inter-fractional uncertainties.

The aim of this work (at University Clinic of Heidelberg) was to assess tissue variations by water equivalent path-length (WEPL) changes and find the dosimetric criteria where corrective actions should be taken i.e. re-optimization of the treatment plan.

Two types of analysis were performed by comparing planning-CT and rigidly co-registered weekly-CTs for 11 patients: A) Dose Forward calculation performed using a research TPS TRiP98, from the treatment plan clinically applied to the patients. The dose evaluation parameters were $V95\%_{PTV}$, $V95\%_{CTV}$ and Gamma-index criteria. B) WEPL maps were generated using the MeVisLab framework to quantify densities variation as a percentage of voxels for the defined range of tissue variation (±3mm H_2O).

Both Gamma-index and $V95\%_{PTV}$ showed tendency to increase or decrease with WEPL variations by strong correlation of 0.73 and 0.6, respectively. A criterion of WEPL as 56% interprets more than 3% variations in $V95\%_{PTV}$ and Gamma passing rate lower than 96.5% (with distance to agreement as 3mm and dose difference of 3%).

The studied method proved to be a prediction tool for physicians in decision making for treatment plan re-optimization need due to inter-fractional density variation, with less computational time and without contouring structures.

Keywords: Charged particle therapy, plan adaptation, pancreas, water equivalent path-length

Table of Content

List of Figures

List of Tables

List of Abbreviations

BB Ball Bearing

BEV Beam's Eye View

CT Computed Tomography

CTV Clinical Target Volume

DOF Degree Of Freedom

DRR Digitally Reconstructed Radiography

DVH Dose Volume Histogram

DTA Distance To Agreement

DD Dose Difference

$\mathbf{D_{min}}$ Minimum Dose

$\mathbf{D_{mean}}$ Mean Dose

$\mathbf{D_{max}}$ Maximum Dose

FWHM Full Width at Half Maximum

GTV Gross Tumor Volume

GSI Helmholtz Center for Heavy Ion Research

GI Gastrointestinal

HLUT Hounse field Look-Up Table

HIT Heidelberg Ion-Beam Therapy Center

HU Hounsfield Units

IMRT Intensity Modulated Radiation Therapy

IGRT Image Guided Radiation Therapy

IES Iso-Energy Slice

IMPT Intensity Modulated Particle Therapy

ITV Internal Target Volume

LEM Local Effect Model

LET Linear Energy Transfer

MRI Magnetic Resonance Imaging

OAR Organ-at-risk

PET Positron Emission Tomography

PRV Planning Risk Volume

PTV Planning Target Volume

PV_{in} Percentage of Voxel within the defined tissue variation range

PV_{norm} Normalized PV_{in}

RBE Relative Biological Effectiveness

RF Radio Frequency

SOBP Spread Out Bragg Peak

SFO Single Field Optimization

TPS Treatment Planning System

VOI Volume Of Interest

V20 Volume received 20% of the prescribed absorbed dose

V80 Volume received 80% of the prescribed absorbed dose

V40 Volume received 40% of the prescribed absorbed dose

V95 Volume received 95% of the prescribed absorbed dose

Chapter 1
Introduction

1.1 Motivation

According to the recent study proposed by World Health Organization (WHO) [1], pancreatic cancer is the twelfth most common cancer in the world and due to its silent behavior usually diagnosed at advanced stages. The new cases diagnosed with pancreatic cancer reached to 338,000 per year and about 277,000 people die each year worldwide due to this disease [2] which sets it to seventh position for being most common cause of death from cancer in the world. Although pancreatic cancer incidence is infrequent, it has the worst survival and mortality rate of all twenty-two common cancers.

Pancreatic cancer is considered as one of the most challenging tumors in the field of oncology due to its decreased prognosis rate. Patients diagnosed with localized pancreatic tumor qualify for resection but their survival rate remained poor due to the high rate of relapse [3]. For locally advanced unresectable pancreatic cancer (LAPC), radiotherapeutic approaches are frequently employed which includes intensity modulated radiation therapy (IMRT) and image guided radiation therapy (IGRT) for conformal absorbed dose distribution and minimum absorbed dose to normal tissues.

It turned out that the use of modern X-rays therapies for pancreatic cancer is limited when dose escalation is desirable and this limitation is mainly due to the surrounding radiosensitive normal organs such as duodenum, stomach, jejunum, liver, and kidneys [4]. Alternatively, charged particles therapy, either proton or carbon, has been considered as a promising alternative due to its explicit advantage; delivering significant dose to the target/tumor while simultaneously minimizing dose to normal tissues [5]. Many researchers have investigated on the aforementioned benefit of proton therapy by comparison with modern X-rays therapies and argued that treatment of pancreatic cancer with proton therapy demonstrates significant reduced absorbed dose to the normal tissues [6,7,8]. Similarly, Japanese studies concluded increased local control and overall survival rate for pancreatic cancers treated with carbon ion therapy [9].

To date, most of the particle therapy facilities have been using broad beams and patient-specific absorbers to conform the dose to the target volume – passive beam delivery system. Moreover, an alternative method has been developed for treatment delivery with high precision – active beam scanning system. This technique allows a pencil beam to raster scan the entire target volume with modulated energy of the beam. At Heidelberg Ion-Beam Therapy Center (HIT), all the pancreatic cancer patients have been treated with this technique either with proton or carbon ion since 2014.

It has been observed [53] that the benefit of scanning systems is usually compromised by the treatment of moving tumors such as pancreatic tumor. Being an abdominal organ, pancreas experiences internal organ motion and respiratory induced motion which causes strong inhomogeneous dose distribution. Furthermore, daily setup errors, tumor shrinkage and bowel motion results in beam range variation. In general, the inevitable inter-fractional motion manifests itself in beam undershoot or overshoot. The above mentioned uncertainties explains explicit requirement of treatment plan adaptation for pancreatic patients treated with charged particle therapy.

1.2 Scope of this Work

Given the fact that organ motion influences the treatment outcome, this might requires re-optimization of the treatment plan. This situation become more critical for patients with abdominal cancer such as pancreatic patients, who are more susceptible to internal organ motion due to extreme bowel movement, weight loss, tumor shrinkage and respiration.

Daily plan adaptation is an advance approach but not as feasible for ion-beam therapy as it is for photon therapy because of the plan complexity and time taken for re-planning. In practical scenario when patients are imaged before treatment delivery, it is difficult to predict how the bowel movement and weight loss will affect the dose distribution and assess the necessity of re-planning.

In this thesis, the intention was to develop criteria (considering the dosimetric tolerances) where corrective action should be taken, therefore, re-optimization of the treatment plan, with less computational work and time consumption.

Chapter 2
Background and Fundamentals

2.1 Background

In the community of radiotherapy researches are striving consistently to improve the quality of treatments and investigate new ways of treating cancer. One such way is to treat cancer with charged particles therapy and its use has been hypothesized to yield improved treatment as compared to photon and electron therapies. The use of charged particles, either proton or carbon, have been shown to be beneficial for pancreatic cancer patients [6,7,8,9]. This chapter presents some basics of particle physics required for the good understanding of this work.

2.1.1 History to Present

The well-known benefit of charged particle therapy, the characteristic inverted depth dose profile with a high local absorbed dose in a well-defined depth (Bragg peak), was first suggested by Robert Wilson in 1946 [10]. The substantial biological and physical advantage of protons was investigated from treating the first human patient with protons beam in the mid-1950s at the University of California Lawrence Berkeley Laboratory [11].

Until 1990 proton facilities were dedicated for research purposes but in the same year the first clinical based proton therapy facility for treatment of cancer patients was built at Loma Linda, USA [12]. In 1992 therapy with carbon ions was first implemented by Japanese in Chiba [13]. According to the Particle Therapy Co-operative Group (PTCOG), there are 57 particle therapy facilities currently operating with a further 33 under construction in the world [14].

2.2 Motivation for Particle Therapy

The rationale for using charged particles in radiotherapy is mainly due to their beneficial physical characteristics in comparison to photons [15] and electrons. Charged particles possess finite range in tissue which helps in dose sparing of critical structures distal to the target volume. The range of charged particle depends on the primary energy and the physical characteristics of target material. Although electrons

possess the same behavior but doesn't represent a well defined Bragg Peak. This phenomenon aided particle therapy to increase the therapeutic window i.e. increasing the probability of tumor control over the damage of surrounding normal structures [16].

2.2.1 Energy Deposition and Absorbed Dose

When a charged particle traverses through matter it ionizes atoms and deposits the energy along its path. The dose is a measure of the amount of energy from an ionizing radiation deposited in a mass of the material; absorbed dose defined by ICRU is [17]:

$$D = \frac{\Delta E}{\Delta m} \tag{2.1}$$

Where ΔE is the absorbed energy to a mass element Δm and its SI unit is gray (Gy).

The dose measurements which are usually performed with air filled ionization chamber should be converted to absorbed dose in water which can be calculated for a parallel beam, with particle fluence F, travelling through a thin layer of absorbing material with mass density ρ, as [59]:

$$D[Gy] = 1.6 \times 10^{-19} \times \frac{dE}{dx}\left[\frac{keV}{\mu m}\right] \times F[cm^{-2}] \times \frac{1}{\rho}\left[\frac{cm^3}{g}\right] \tag{2.2}$$

Where dE/dx is the energy loss of particles per unit path length i.e. stopping power or specific energy loss.

2.2.2 Stopping Power

Stopping power is the rate of energy loss per unit of path length by a charged particle of a specific kinetic energy in a medium of atomic number Z. When a deep located tumor needs to be irradiated, e.g. 30cm depth, it would require ion beam range corresponding to specific energy up to 220 MeV/u for protons and 430 MeV/u for carbon ions. Since the slowing down process, describing by the stopping power, is dominant by inelastic collision with the target electrons of the incident medium, it is expressed by the Bethe-Bloch formula [18]:

$$-\frac{dE}{dx} = \frac{4\pi e^4 Z_t Z_p^2}{m_e v^2}\left[ln\frac{2m_e v^2}{< I >} - \ln(1-\beta^2) - \beta^2 - \frac{C}{Z_t} - \frac{\delta}{2}\right] \tag{2.3}$$

Here Z_p and Z_t are the nuclear charges of the projectile and target, m_e and *e* are the mass and charge of the electrons respectively, <I> is the mean ionization energy of the target atom, C/Z_t is a shell correction term and the density correction term is δ/2.

2.2.3 Bragg Peak and Spread Out Bragg Peak

The entrance dose of the charged particles is comparatively lower than for photons and demonstrates dose escalation in distal region followed by a very steep dose fall-off to almost no dose. Charged particles ionization density increases with increased depth which results in deposition of majority of the energy at a certain depth in a material. This narrow region of increased ionization density at the end of the charged particles range is known as Bragg peak. In figure 2.1 the behavior of charged particles, proton and carbon, is compared to the photon depth dose curve.

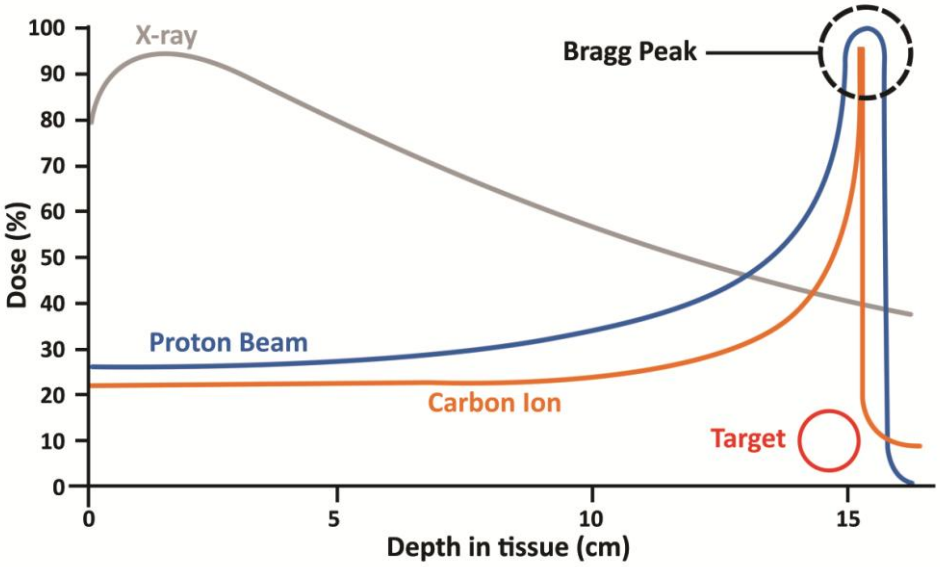

Figure 2.1: Depth-dose profile of photon, proton and carbon ions

The large mass difference of charged particle from atomic electrons makes them able to traverse in almost a straight line due to small deviations caused by atomic electrons. The depth of Bragg peak primarily depends on the initial energy of the particles, thus the charged particles beam has increased penetration depth as the incident beam energy increases.

In order to cover the entire depth of the target volume with uniform absorbed dose, charged particles energy should be modulated to cover a spectrum of energies. For this purpose, a spread out Bragg peak (SOBP) can be achieved if multiple monoenergetic Bragg peaks are superimposed to yield conformed uniform dose to the target whilst sparing critical structures present distally. This phenomenal effect of SOBP results in high absorbed doses to the proximal area of the target in comparison to single Bragg peak, however, significantly less than in photon irradiation.

2.2.4 Range Straggling

The path length is the distance that a charged particle travels before coming to rest. The range is defined as the mean path length of a set of charged particles of the same incident initial energy. Range straggling is responsible for the alteration in the individual path lengths and is due to the stochastic nature of the interactions that occur. The mean range R(E) can be related to the mass stopping power through equation 2.3 as [19]:

$$R(E) = \int_{E}^{0} \left(\frac{dE'}{dx}\right)^{-1} dE' \tag{2.4}$$

The behavior of heavy ions has been demonstrated as in figure 2.2, where protons shows more range fluctuation as the energy increases, but much heavier ions like carbon have very less variation because heavy ions are very less scattered and travel almost on a straight line.

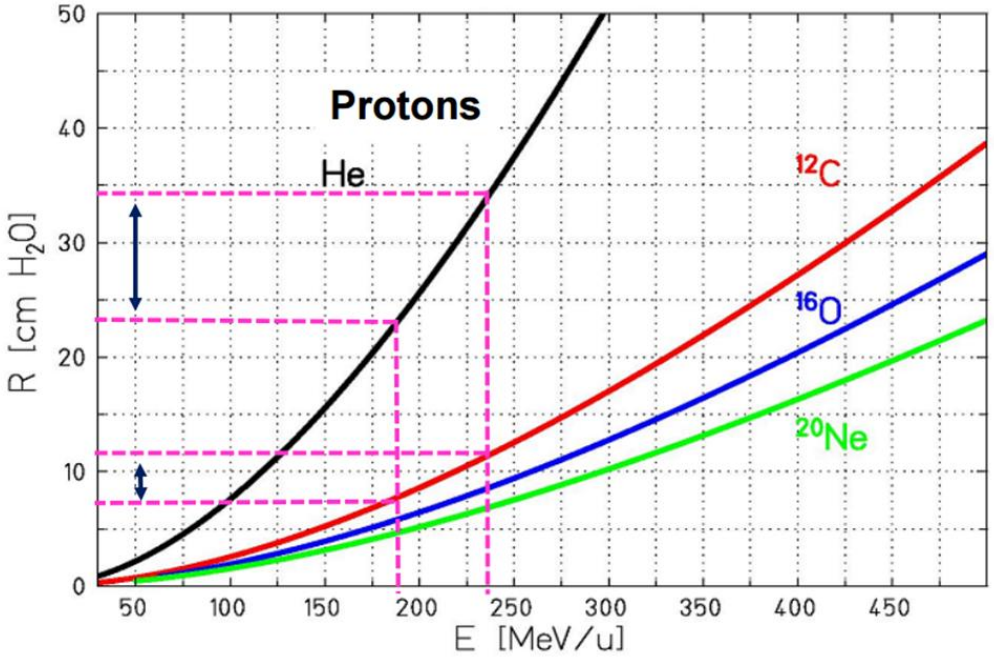

Figure 2.2: Mean range of ions in water. The mean range of protons is higher than that of carbon at the same energy (shown by pink dashed lines) [19]

2.2.5 Lateral Scattering

When a charged particle traverses through an absorbing material it undergoes a lateral deflection while penetrating. This beam spread is primarily due to the Coulombs interactions with the target nuclei. The amount of deflection depends on the type of particle and its energy, for example carbon ions spreads less than protons

because they are heavier which makes carbon ions clinical superior for offering sharp dose gradients i.e. reduced doses to organ at risk (OAR) [20].

2.2.6 Nuclear Fragmentation

A certain fraction of protons have nuclear interactions in tissue, mainly with ^{16}O (about 1% per cm of all protons in a beam) [21]. The nuclear interactions cause a decrease in primary proton fluence and lead to secondary particles absorbed dose such as neutron but the absorbed dose from these nuclear interactions is negligible in the Bragg peak. Instead, ions (heavier than protons) with energies of several hundreds of MeV/u possess significant contribution from nuclear interaction to absorbed dose and manifest itself as a dose tail at the distal end of the depth dose profile (for example carbon ions), see figure 2.1.

2.2.7 Biological Effect

In order to relate the biological effects from different types of radiation the relative biological effectiveness (RBE) is used. The RBE is dependent upon the absorbed dose, absorbed dose rate, fractionation and the irradiated tissue irrespective of the radiation type. RBE is defined as the ratio of the absorbed dose from the reference radiation (photons) and the absorbed dose from the other radiation type producing the same biological effect.

Protons possess slightly (10%) higher biological effects than that of photons. The generic approximation for the RBE value used for clinical proton beams is 1.1 [22] which means the protons will result in slightly higher damage to the tissues than the same dose of photon beam. Protons linear energy transfer (LET) increases with depth and so the RBE, however studies shows that RBE value varies between 1.1 (at the entrance of the beam) and 1.6 (at the distal edge of the Bragg peak) [23]. This variation could result in increase of protons effective range by few millimeters compared to the physical range. The aforesaid effect will have significant impact on treatments and organs at risk (OAR) close to the tumor although it is rarely taking into account at any proton therapy center.

Carbon ions are superior to protons in terms of enhanced RBE which could also vary from 1 to 5 [24]. Similar to protons, high energy carbon beam demonstrate low RBE at the entrance of the beam and a high RBE in the target volume therefore the side effects to normal tissues are small whilst retaining maximum effect to target volume. Due to large variation in RBE of carbon ions, simple approximation is not

appropriate. A biological model, local effect model (LEM), has been developed to predict the RBE in mixed radiation field (combination of different energies of particles) [52]. Although, there are improved versions of LEM which have been established named LEM II and LEM III [25]. Other than LEM, there are different biological models also available to account with the biological effects for example the micro-dosimetric kinetic model (MKM) [54].

2.3 Charged particle Accelerators & Beam Transport System

2.3.1 Production

Protons can be accelerated to produce a beam of sufficient intensity and energy by two primary methods, through the use of either a cyclotron or a synchrotron. The intensity should be high enough to deliver the treatment in a short period of time usually targeted around 2-3 minutes [26]. The proton energy should be in the range of 160 to 250 MeV which is necessary to deliver SOBP beams for a broad range of tumor depths. On the other hand, to accelerate carbon ions synchrotron is used.

The cyclotron is a relatively simple particle accelerator, usually producing particles at a fixed energy, from the centre along a spiral path, which then has to be appropriately modified to make it suitable for treatment. Cyclotrons use two opposing evacuated dees separated by a gap in which an alternating electric field is applied [48]. Protons are accelerated in increasing orbits in response to the electric field each time they pass in-between the dees until the desired kinetic energy is achieved. A static magnetic field oriented perpendicular to the orbit of the protons acts to keep the protons focused in orbit until exiting the cyclotron. Energy degraders are used as needed to reduce the proton energy after the beam has exited the cyclotron.

Synchrotrons, cyclic particle accelerator, can in principle produce beams of almost any energy up to the maximum, but because they are pulsed machines, it delivers the dose rather slowly, leading to reasonable longer treatment times and increased patient discomfort. A synchrotron requires the use of a “primary” linear accelerator to provide a source of 3 to 7 MeV protons to then further accelerate [26]. The protons are then accelerated in a ring of constant radius and kept focused in the desired orbit by the use of multiple bending magnets. The strength of the magnetic field and the radio frequency (RF) are increased as also the proton continuously gains in kinetic energy [26]. For this reason, a synchrotron can produce beams of variable

energy, consequently, and in contrast to a cyclotron, do not need energy degraders to produce a SOBP.

2.3.2 Beam Delivery System

The beam transport system is actually the connection part between the accelerators and treatment rooms. It is used to transfer the beam from the outlet of the accelerator to the entrance of the treatment rooms. Beam delivery systems are typically defined as either passive or active, depending on how the beam is conformed to the target. In the following both active and passive delivery systems are explained in detail.

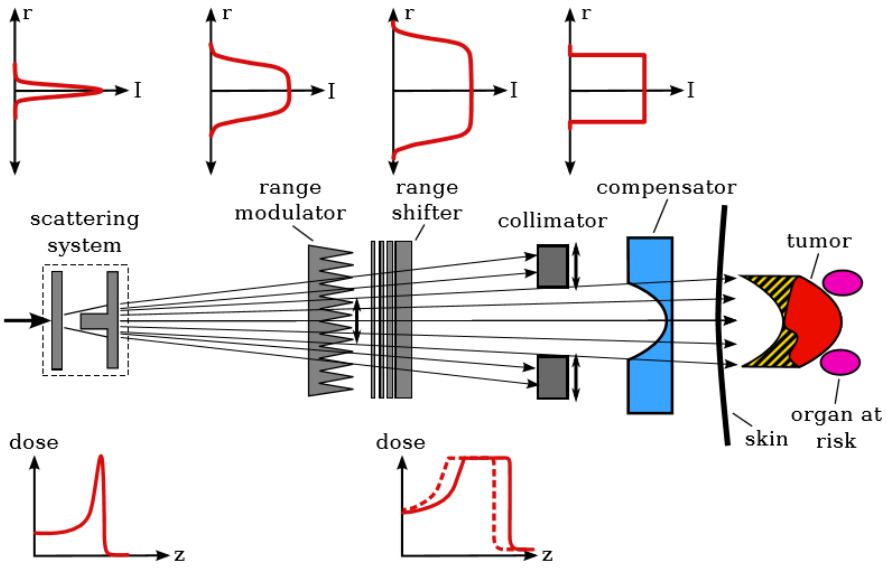

Figure 2.3: Illustration of a passive beam delivery system. The narrow, mono-energetic beam is broaden by a scattering system to match the required lateral dimensions. Lateral and longitudinal adaption to the tumor is performed by different passive modulator devices. The distal edge of the tumor is conformed by an individually machined compensator which also results in unwanted dose to normal tissue (hatched area) [19].

Passive system

Passive system provides conformity in the target by scattering and degrading the primary beam using various beam shaping devices as shown in figure 2.3. Beam modulation is required so as to achieve absorbed dose homogeneity in depth which could be accomplished by varying the thickness of absorber material through which the beam will travel therefore ridge filter or range modulator wheel are used [27]. Initially, a pair of scattering foil, help in increasing the width of the primary beam, then blocks and apertures are used to collimate the beam produced by the scatters, to the required target shape. Finally, a customized patient specific compensator is used to shape the dose distribution to the distal edge of the tumor volume. This technique has

a limitation because it conforms the proximal edge of the target in a similar manner as it conforms the dose to the distal edge of the target volume which results in full dose to the normal tissues.

Active system

This system uses magnetic fields to scan the particle beam laterally across the target. Additionally also gives a capability to change the energy which allows conformality in three dimensions as shown in figure 2.4. There are two methods of beam scanning [28,29]: spot scanning and continuous scanning, for both the irradiation is delivered as a series of 2D layers. Spot scanning delivers the dose in finite steps, after delivering each beam it is switched off while the elements which steer the beam are reconfigured (changing beam position or energy) to deliver the dose to the next spot. According to ICRU, the spot positions should be separated by less than 80% of the beams full width half maximum (FWHM) to ensure homogeneous absorbed dose distribution [30]. The small separation among spots could reduce the sensitivity to fluctuations in the pencil beam position but increases the treatment time. The primary difference in spot and continuous scanning is that the beam remains on in continuous scanning when the position needs to be changed and each layer is irradiated, but it will be interrupted while changing the beam energy and turned on back for the next layer, this process will be repeated until the whole target has been fully irradiated. In figure 2.4 a raster scanning system has been demonstrated in which the beam dose is delivered in layers of same thickness and each layer will correspond to a specific energy (iso-energy slices, IES).

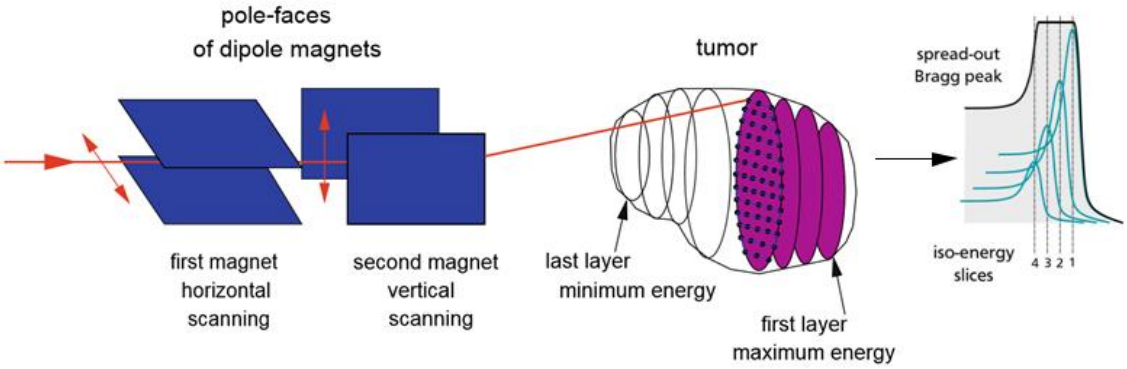

Figure 2.4: Illustration of an intensity controlled magnetic scanning system in irradiating the target volume slice by slice with a moving pencil beam; sufficient overlapping is maintained to yield a homogeneous target absorbed dose in the longitudinal dimension (SOBP). [31].

2.4 Treatment Planning

In radiation therapy treatment planning is a major step which includes all the concepts explained above. This usually starts with acquiring a Computed Tomography (CT) for anatomical patient information; this has to be done without contrast agents (with different densities) to correctly calculate the range of the particles and the dose deposition in tissue (tumor and normal function tissue). Later other imaging modalities are used such as magnetic resonance imaging (MRI) and positron emission tomography (PET) to aid in better delineation of target and organs at risk (OAR) volumes segmentation.

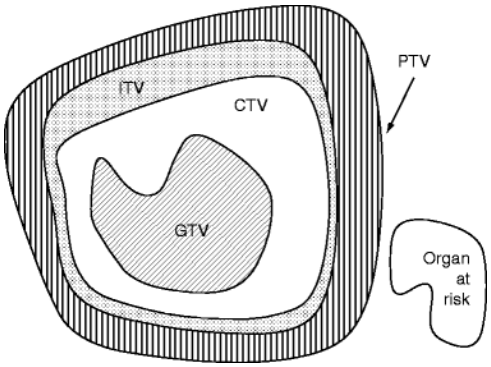

Figure 2.5: Representation of the ICRU volumes for treatment planning. CTV clinical target volume, GTV gross tumor volume, ITV internal target volume, PTV planning target volume [32]

Gross Tumor volume: The GTV is the gross palpable or visible/demonstrable extent and location of malignant growth.

Clinical Target Volume: The CTV is a tissue volume that contains a demonstrable GTV and/or subclinical microscopic malignant disease, which has to be eliminated. This volume thus has to be treated adequately in order to achieve the aim of therapy, cure or palliation.

Internal Target Volume: This is the margin that must be added to the CTV to compensate for expected physiological movements and variations in size, shape, and position of the CTV during therapy.

Planning Target Volume: The PTV, is a geometrical concept, and it is defined to select an appropriate beam size and beam arrangements, taking into consideration the net effect of all the possible geometrical variations, in order to ensure that the prescribed absorbed dose is actually in the CTV.

Organs at risk: Organs at risk (OAR) are normal function tissues whose radiation sensitivity may significantly influence treatment planning and/or prescribed absorbed

dose. Although the volume which includes margin around OAR that accounts for movement is called planning risk volume (PRV).

After making a tridimensional (3D) model of the contoured structure the most suitable beam configuration has been defined (typically 1 or 2 beams in particles therapy) and dose distribution is adapted to the planned target/tumor volume; according to ICRU, 100% of the PTV volume should receive between 95% and 107% of the planned absorbed dose [33]. Beyond this step, treatment planning should incorporate the physical interactions of the particles in the tissue, algorithms and the biological model developed for absorbed dose calculation. This step requires inverse planning technique which optimizes the desired absorbed dose distribution and incorporates particle fluence while sparing OAR with proper dose constraints. However, a raster scanning system would require several scanning position to attain a homogeneous absorbed dose distribution for the target/tumor volume, in other words, for the application of Intensity Modulated Particle Therapy (IMPT) it incorporates superposition of the pencil beams with individual energy, position and particle number and yields a biologically effective dose distribution. On the other hand, the second approach is to optimize the weights on a field-by-field basis, that is, each field is optimized individually to deliver a fraction of the prescribed doses to the entire target/tumor volume. This method is called single-field optimization (SFO) [55].

Later the Treatment Planning System (TPS) performs the absorbed dose calculation based on the anatomical information from the patient CT imaging which contains information about electron density distribution (representing X-ray attenuation) in the human body given in Hounsfield (HU) values. The relationship of CT number and stopping power [56, 57] is a helpful measure to calculate the dose in a heterogeneous medium deposited by the Bragg peak. In order to relate the travelling behavior of a charged particle with a CT voxel (representing HU), where voxel is a 3D form of pixel, corresponding to path length in water, a concept has been introduced as water equivalent path length (WEPL). For this purpose, Hounsfield units Look-Up Tables (HLUT) have been used in treatment plan optimization and absorbed dose determination. The HLUT is estimated by measuring HU values and particle ranges (WEPL) of tissue-equivalent materials using the stoichiometric method [58]. Lastly, absorbed dose optimization process assigns raster points to each layer with specific energy and spacing defined earlier to cover the target in water equivalent space.

2.5 The Heidelberg Ion-Beam Therapy Center

At Heidelberg Ion Therapy (HIT) facility the first patient was treated in 2009 with particle therapy. HIT is a part of the University clinic of Heidelberg based on the pilot project initiated at Helmholtz Center for Heavy Ion Research (GSI) [34]. This facility has three clinical beam-lines, two of them are horizontal and one with a gantry (figure 2.6) to allow different beam directions and was the worldwide first heavy ion gantry (isocentric) with beam scanning capabilities; however other two horizontal beams also provide beam scanning function. The ion energy ranges from 50 to 430 MeV/u corresponds to ion penetration depths of 20 to 300 mm in water [35]. To date, HIT have been using protons and carbon ions for the clinical purpose although helium and oxygen ions are also available but limited to research purposes. At HIT facility, TPS *Syngo (RT Planning* by Siemens) have been used for clinical purpose however a research treatment planning system TRiP98 [36] is also available. Both incorporate the necessary requirements of a treatment planning software as explained in section 2.4. Moreover a positron emission tomography and a CT machine (PET/CT) have been installed so as to evaluate the range of ions.

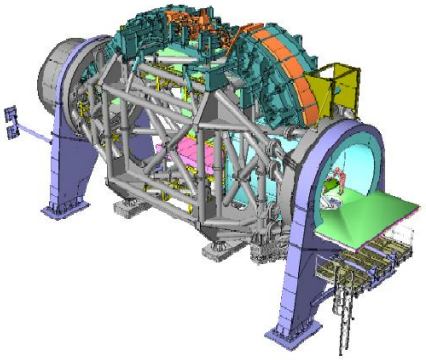

Figure 2.6: Drawing of the heavy ion gantry at the HIT, including mechanics, beam line components and patient treatment room (MT Mechatronics) [35]

2.6 Motion Impact on Treatment Delivery

In the field of radiation therapy patient motion, either inter or intra-fractional, have been a major hurdle for the accurate delivery of treatment. Moreover the fact of using a beam scanning system turns motion issues more dominant. The anatomical site such as gastrointestinal (GI) system is susceptible to motion influences on the treatment outcome and workflow requires changes in treatment planning dosimetry and delivery. The inter-fractional motion affects the treatment in a matter of minutes to hours, thus requires interventions at the beginning of the treatment. The motion effect in the treatment of pancreatic patients is usually comprised of patient daily positioning and setup errors, internal organ motion such as tumor motion due to breathing effect

(intra-fractional motion) and changes in bowel movement (inter and intra-fractional), weight loss during the course of treatment and tumor shrinkage effect along the treatment [37].

As far as patient positioning and setup errors are concerned, radiation therapy community have already investigated and established the state of the art immobilization systems and techniques which have been implemented in particle therapy as well. Therefore this study will concentrate on the other factors of inter-fractional motion mentioned above assuming that patients were precisely localized and immobilized during treatment, although one has to realize there is always a possibility for further improvement.

When we relate the effect of inter-fractional motion with particle therapy, it has been found that motion causes density heterogeneities which will not only affect the shape of the Bragg peak but also the position due to the range of particles, this effect can be seen in figure 2.7.

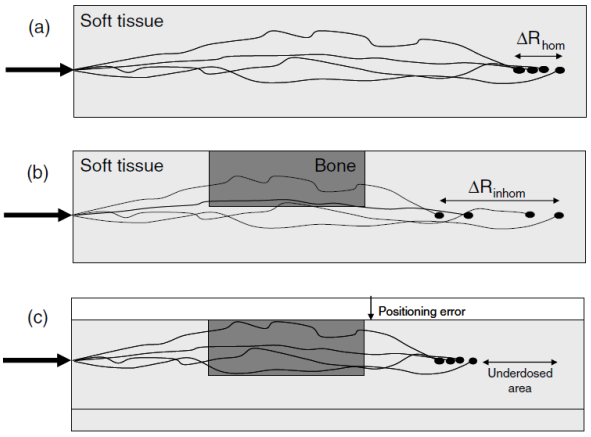

Figure 2.7: The effect of density variation along the beam path has been demonstrated. (a) Proton tracks through a homogenous medium. (b) Similar tracks through a heterogeneous medium. (c) Same tracks through a shifted version of the density heterogeneity [38].

One of the common approaches for reducing the inter-fractional motion is adaptive therapy. For this purpose image guided techniques and re-optimization of dosimetry plans have been implemented to retain the dosimetric quality throughout the treatment course. As far as photons are concerned, plan adaptation strategy [39] is now being commonly used at some facilities but in particle therapy it is still a challenging step because of the time consumption due to complex treatment planning and delivery techniques. Even if the aforementioned factor has overcome, there is always the question ‘when is certainly needed plan adaptation?’ because there is no standard definition for such situations.

Chapter 3

Plan Quality Assessment

3.1 Introduction

This chapter explains the dose calculations performed on a dataset of patients. It also provides an overview of treatment planning dosimetry performed on pancreatic patient at HIT and the use of research planning system for dose forward calculations on these patients. A complete detail has been shown about the patients included in this study regarding absorbed dose prescription, fractionation, field setups and chosen particle for therapy. Further dosimetric parameters have been defined for the evaluation of the treatment dosimetry plans and the results of those parameters have been discussed in detail. The impact of absorbed dose distributions on OARs has also been summarized in this chapter.

3.2 Materials and methods

3.2.1 Patient Cohort

For this work (a retrospective study), eleven pancreatic patients were selected who were treated with scanned ion beam therapy including both carbon ions and protons at HIT facility from 2014 to 2016. Table 3.1 explains details of the patients regarding chosen particle for therapy, dose prescription, fractionation, field setups and number of weekly-CTs available.

3.2.2 Patient Workflow

In the following, patient workflow has been described for the patients included in this study:

Patients positioning and immobilization: Patients were positioned prone on vacuum mattress, hands were raised above their head and feet were resting on a bolster, shown in figure 3.1. The skin marks were placed which will help in daily positioning.

Planning CT: For treatment planning, a free-breathing CT (Somatom Sensation Open CT scanner by Siemens) covering from diaphragm to iliac crest was acquired without contrast. Additionally, a CT with contrast agent and a 4DCT (based on respiratory

gating) are acquired in combination with CT to allow a better definition of the target volume and organs at risk.

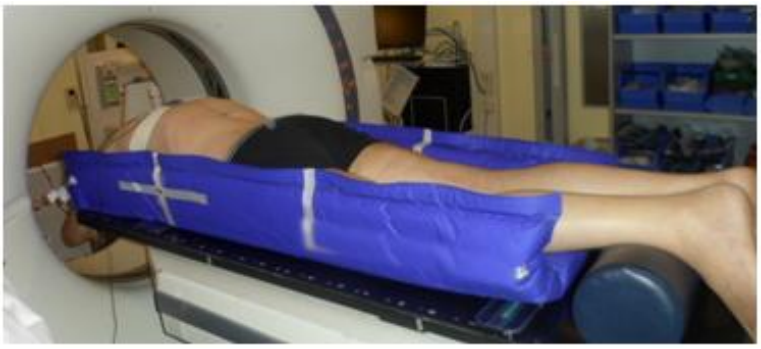

Figure 3.1: Patient positioning and immobilization for pancreatic treatment patients of this study

Particle selection: Ten patients were treated for proton beams and only one patient with carbon ion beam, refer to Table 3.1. The selection criteria for proton over carbon ions and vice versa depend on physician's practice.

Patient	Particle	Dose (GyE)/fr	No. of Weekly-CT	No. of Fields and Setup (refer to figure 3.2)
A	Proton	1.8 / 25	5	2; Setup A
B	Proton	1.8 / 25	3	2; Setup A
C	Proton	1.8 / 25	3	3; Setup B
D	Proton	1.8 / 25	3	2; Setup A
E	Proton	1.8 / 25	3	2; Setup A
F	Proton	2 / 27	3	2; Setup A
G	Proton	1.8 / 25	3	2; Setup A
H	Proton	1.8 / 25	4	2; Setup A
I	Carbon	4 / 12	1	2; Setup A
J	Proton	1.8 / 25	5	2; Setup A
K	Proton	1.8 / 25	6	2; Setup C

Table 3.1: Details of all the patients included in this study: particle selection, absorbed dose per fraction, number of weekly-CTs and treatment field configuration

Treatment planning: All treatment plans were planned using TPS *Syngo (RT Planning* by Siemens), refer to section 2.4, using IMPT technique with iso-energy slice

(IES) of 3 mm and full width at half maximum (FWHM) of 10 mm for carbon ions, 3mm IES and 8 mm FWHM for protons. Dosimetry plans were optimized to cover the PTV with homogenous absorbed dose and simultaneously reducing the dose to the OARs to the clinical dose constraints.

Field setup: In this study nine out of eleven patients had two posterior oblique fields (figure 3.2 setup A). The other two patients were planned with different geometries to reduce the dose in kidney and bowel OAR, hence one patient had right lateral and a posterior field (setup C) and one patient had two posterior oblique and a posterior field (setup B). The field setups for all the patients are described in Table 3.1 and shown in figure 3.2.

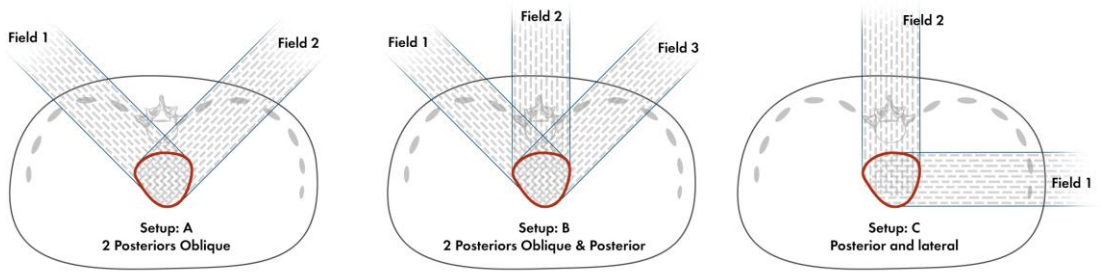

Figure 3.2: Different field configuration used for the patients included in this study

Dose prescription: For proton beam therapy, the typical dose regime used is 45 GyE in 25 fractions and 9 GyE in 5 fractions for a boost volume. This research work does not include the evaluation for the boost plan. For the patients included in this work, dose fractionation is summarized in Table 3.1. In the following all the dose values are given in GyE referring to weighted dose by relative biological effects (RBE) for protons and carbon ions.

Patient position verification and treatment delivery: Before treatment delivery, patients are aligned using skin marks with laser and this setup is verified with orthogonal X-ray images acquired in the treatment room related with the (initial) planning-CT. Those images then are compared with Digitally Reconstructed Radiograph (DRR) for bony anatomy alignment and corrective measures taken as per need. After alignment adjustments, treatment is delivered according to the dosimetry plan.

Weekly-CT: Each patient was scheduled for follow-up weekly-CTs however resulting in a different number of weekly-CTs for the whole treatment course; this detail is described in table 3.1. These CTs were performed using the PET/CT scanner (Siemens Biograph mCT, Siemens Molecular Imaging). In this study, the total number

of weekly-CTs acquired was 39 from 11 patients. The weekly-CTs were performed in accordance with the planning-CT, same patient positioning, free-breathing and without contrast.

3.2.3 Image Registration

Weekly-CTs acquired from each patient were registered with their respective planning-CT using 3D slicer platform software [40]. The rigid registration approach was used as it aligns images of the same subject acquired at different times in the clinical routine. Rigid registration gives 6 degree of freedom (DOF) which consists of 3 translations and 3 rotations. The transformation mapping was done by keeping Planning-CT image as fixed image (reference) and weekly-CT image as moving image (target). The landmarks matching criteria included bones i.e. vertebral column and ball-bearing (BB) fiducials which were placed on patient skin for alignment at the time of scanning.

3.2.4 Contoured Volumes

In the following, the contoured volumes have described which were used for planning-CT and weekly-CT plan doses evaluation:

Target volume: For forward absorbed dose calculation the target volumes including GTV, CTV, ITV and PTV were transferred from the TPS Syngo *(RT planning by Siemens)* and applied to the planning-CT and respective weekly-CTs.

Group A	Group B	Analyzed OARs
Redrawn OARs used for weekly-CTs	OARs used for weekly-CTs as used in planning-CT	Spinal Cord, Left kidney, Right Kidney, Bowel
Patient A	Patient F	
Patient B	Patient I	
Patient C	Patient J	
Patient D	Patient K	
Patient E		
Patient G		
Patient H		

Table 3.2: Details about contoured OARs for weekly-CTs

Organs at Risk (OAR): Table 3.2 contains details about the contoured OARs for weekly-CT of all the patients. There were seven out of eleven patients who had new OAR drawn per weekly-CT which was useful for dose evaluation. For other four patients same OARs were used for the weekly-CTs as were drawn for planning-CT. In this study the dose evaluation of OAR was limited to only 3 organs: spinal cord, both kidneys and bowel, as expressed in Table 3.2.

3.2.5 Absorbed Dose Calculation

As stated in the section 2.4, planning-CTs were optimized and calculated on a commercial TPS. For this purpose, the dose distribution of weekly-CTs and planning-CTs were forward calculated using TRiP98. Thus the dose distributions correspond to the same clinically applied to patients with the aim to cover the CTV with the prescription absorbed dose.

Plan assessment parameter: The dose evaluation parameters were set as volume of CTV received 95% dose ($V95\%_{CTV}$), volume of PTV received 95% of dose ($V95\%_{PTV}$), PTV maximum dose, PTV minimum dose (D_{min}) and PTV mean dose to (D_{mean}).

For dose plan comparison purpose gamma-index has been used since it is more sensitive to high and low dose gradients regardless of the contoured volumes. It is a single metric for dose maps that combines features of both dose difference (DD) and distance to agreement (DTA), see equation (3.1). It quantitatively compare both the planning-CT ($\vec{r}_{plan}$) and weekly-CT ($\vec{r}_{ct}$) dose distributions in terms of dose values and their positions, respectively with the acceptance criteria in this research work of 3% dose difference and 3mm distance to agreement [41].

$$\gamma(\vec{r}_{plan}, \vec{r}_{ct}) = \sqrt{\frac{\left|\vec{r}_{plan} - \vec{r}_{ct}\right|^2}{DTA^2} + \frac{\left|D(\vec{r}_{plan}) - D\ (\vec{r}_{ct})\right|^2}{DD^2}} \tag{3.1}$$

For the results, a gamma distribution and gamma passing rate was computed using Plastimatch open-source software [42]. This was a helpful tool for the assessment of high dose region of OARs and low dose regions within target volume.

3.3 Results – Absorbed Dose Distribution

3.3.1 Plan Quality Parameters

In the following, dosimetric parameters were evaluated from the dose distributions of planning-CT and weekly-CTs. For comparison $V95\%_{PTV}$ variation was calculated for all the weekly-CTs to their respective planning-CT as shown in figure 3.3. In figure 3.4 the mean and standard deviation for $V95\%_{PTV}$ has been demonstrated for all patients.

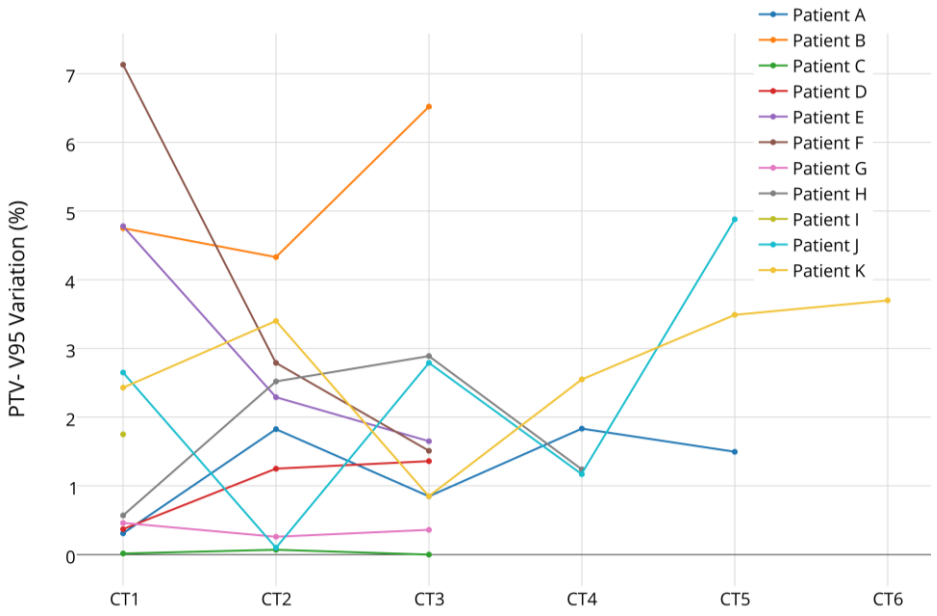

Figure 3.3: $V95\%_{PTV}$ variation along the weekly-CTs for all the 11 patients in reference to planning-CT

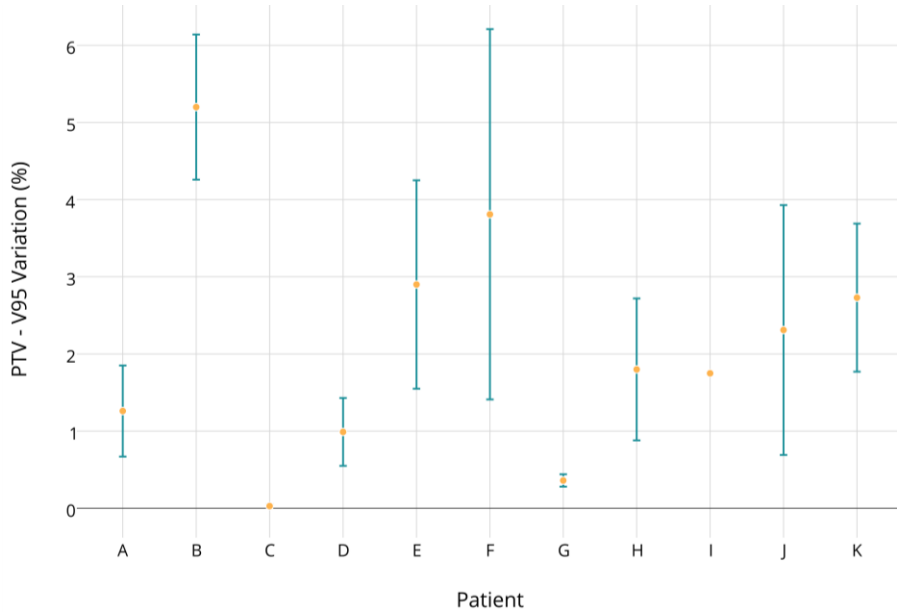

Figure 3.4: Mean and standard deviation of $V95\%_{PTV}$ variation over weekly-CTs represented individually for all the 11 patients

It was observed that only one patient had almost zero variation of PTV coverage for all the weekly-CTs. There were 6 out of 11 patients who had $V95\%_{PTV}$ variation within 3% along the treatment. For worst case the variation was up to 7% which was observed even for first weekly-CT. For some cases maximum variation was observed for first weekly CT and minimum variation for last weekly-CT, for example patient E and patient F in figure 3.3. On the other hand, there were few cases where aforesaid effect was reversed for example patient B and patient D. The complete result can be seen in appendix, table A.1(a).

The deviation of the maximum dose within the PTV was evaluated for all the patients and demonstrated in figure 3.5.

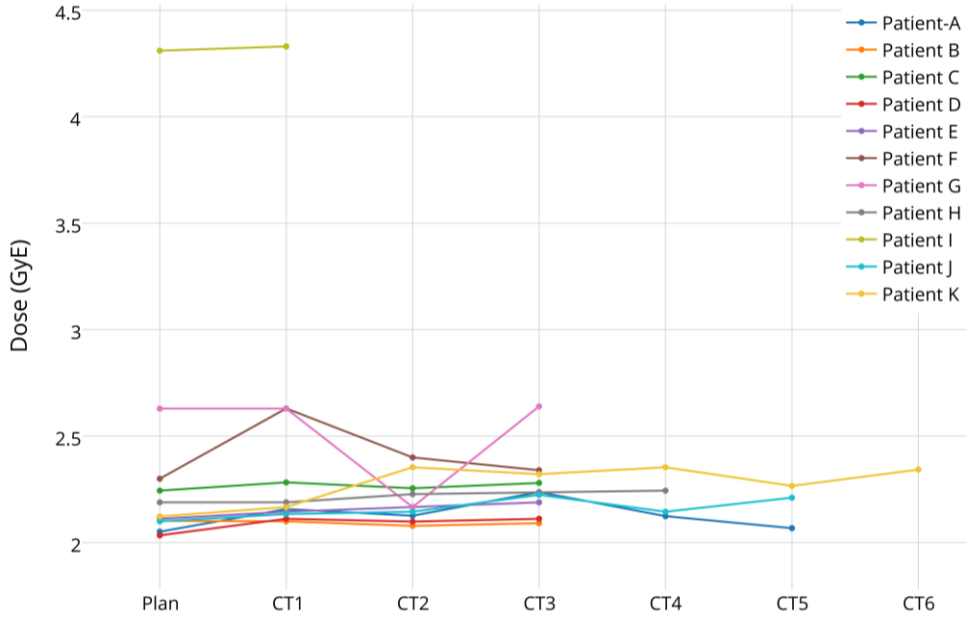

Figure 3. 5: PTV Maximum dose along the weekly-CTs for all the 11 patients in reference to planning-CT (since patients have different dose per fraction, refer to table 3.1)

The dose per fraction is different for each patient for that reason refers to table 3.1 for the details. For most of the patients, PTV maximum dose remained consistent along the weekly-CTs while comparing with their respective planning-CT. The maximum variation was of 0.5GyE and minimum was of 0.02GyE. The major deviation was observed for those patients who had worst $V95\%_{PTV}$ for the weekly-CTs, for example patient F and patient K in figure 3.3 and figure 3.4. However patient G represented high deviation even with minimum $V95\%_{PTV}$ variation as shown in figure 3.3 and figure 3.5. In figure 3.6 the mean and standard deviation for the maximum dose of PTV has been demonstrated for all patients. The complete result can be seen in appendix, table A.1(a).

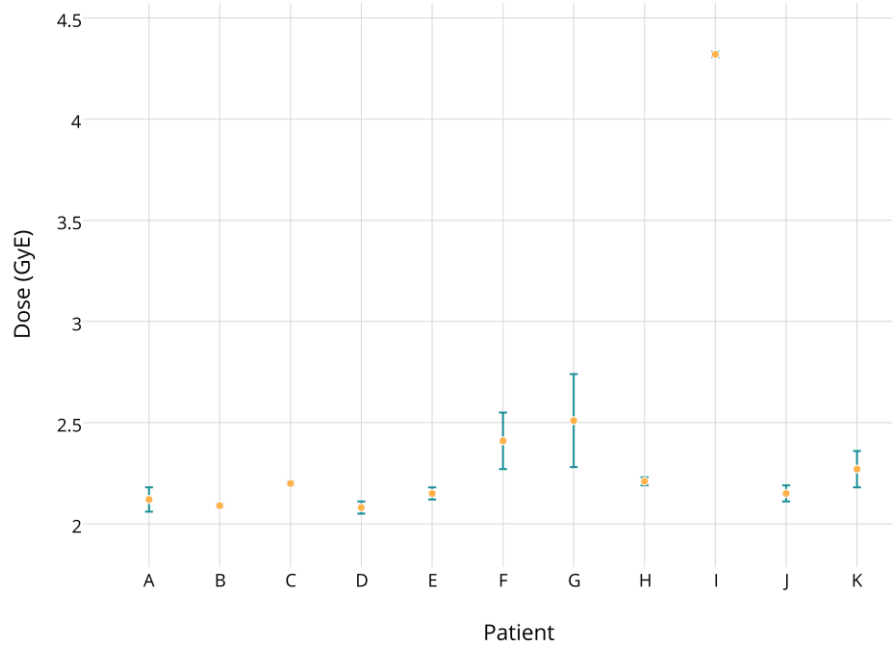

Figure 3. 6: Mean and standard deviation of PTV maximum dose represented individually for all the 11 patients. Note patient I refers to the carbon-ion patient, with dose per fraction 4GyE.

The deviation of D_{min} within the PTV was evaluated for all the patients and demonstrated in figure 3.7.

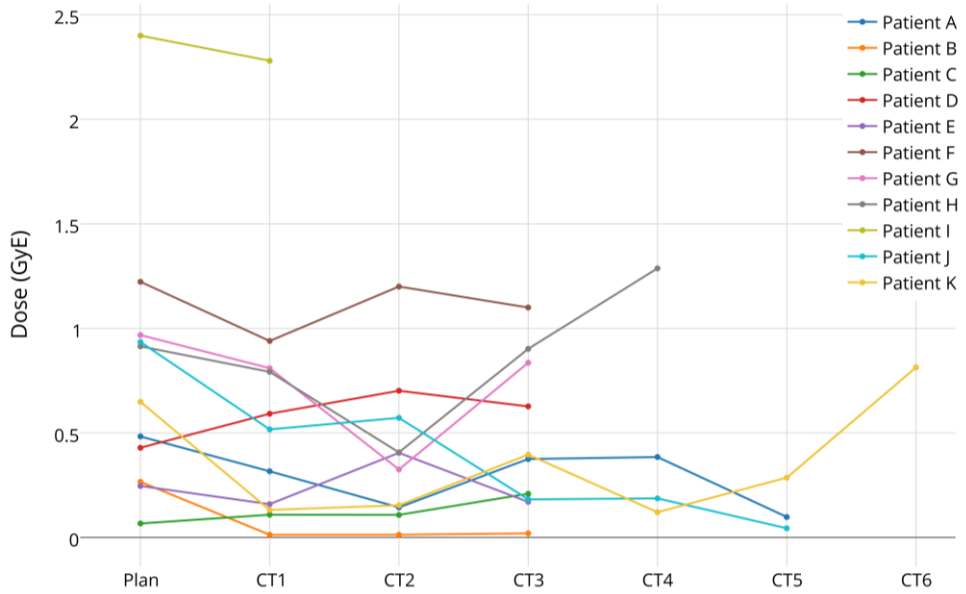

Figure 3.7: PTV D_{min} along the weekly-CTs for all 11 the patients in reference to planning-CT (since patients have different dose per fraction reader is referred to table 3.1)

There were 4 out of 11 patients who had D_{min} lower than 0.5GyE for all the CTs. There were considerable deviations of D_{min} for all the patients along the treatment course. For example, patient B had increased $V95\%_{PTV}$ variation as shown

in figure 3.3 and also represents D_{min} almost zero for all the weekly-CTs. While comparing with plan D_{min} to the weekly-CTs, the maximum variation for D_{min} was of 0.6GyE and minimum variation was of 0.01GyE. In figure 3.8 the mean and standard deviation for the PTV D_{min} has been demonstrated for all patients. The complete result can be seen in appendix, table A.1(a).

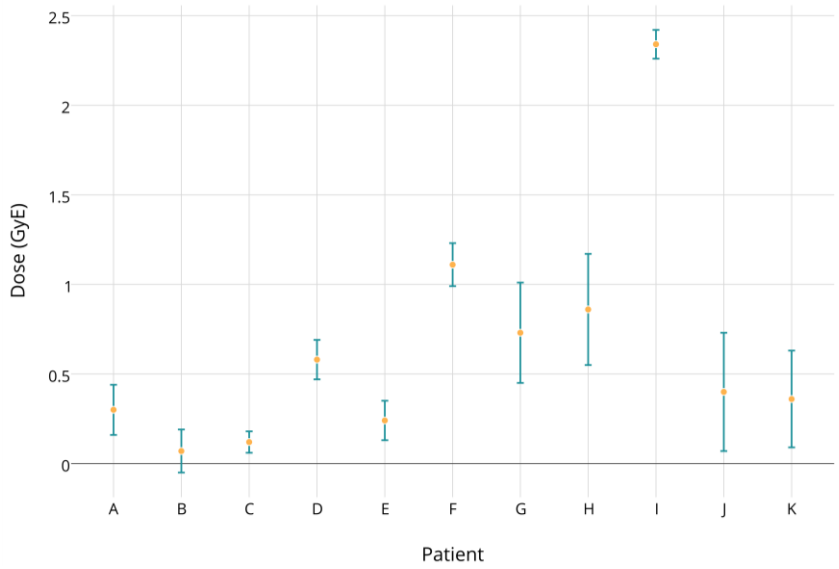

Figure 3.8: Mean and standard deviation of PTV D_{min} represented individually for all the 11 patients

The deviation of D_{mean} within the PTV was evaluated for all the 11 patients and demonstrated in figure 3.9. For all the patients PTV D_{mean} was fairly consistent in comparison with D_{min} and PTV maximum dose.

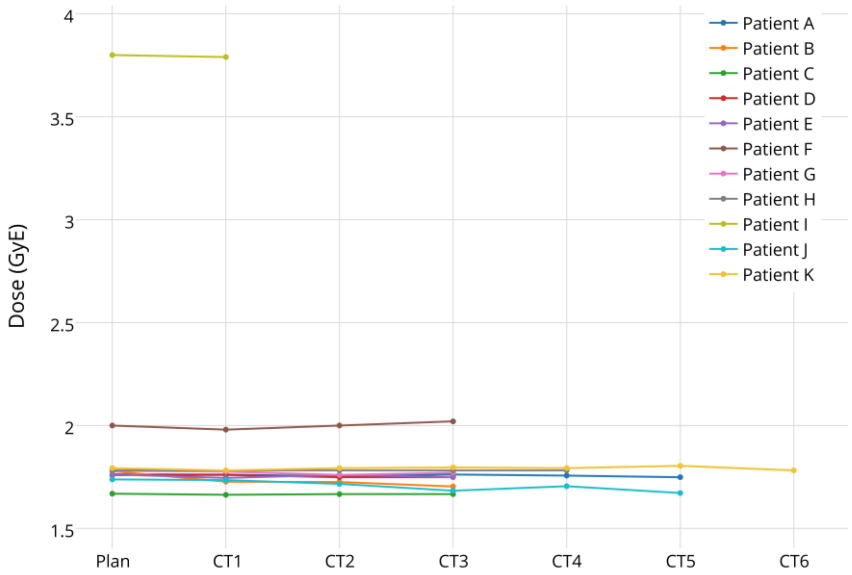

Figure 3.9: PTV D_{mean} along the weekly-CTs for all the 11 patients in reference to planning-CT (since patients have different dose per fraction reader is referred to table 3.1)

For comparison, $V95\%_{CTV}$ variation was calculated for all the weekly-CTs to their respective planning-CT as shown in figure 3.10.

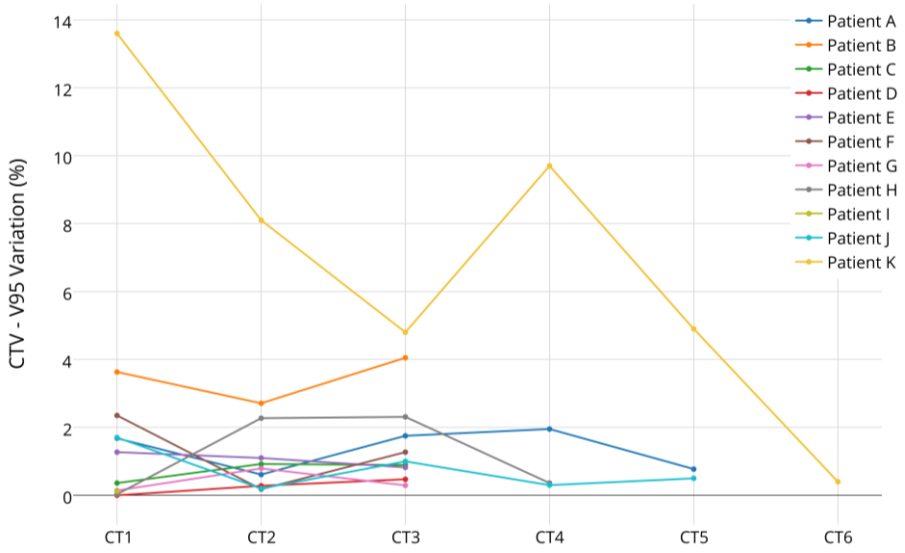

Figure 3.10: $V95\%_{CTV}$ variation along the weekly-CTs for all the 11 patients in reference to planning-CT

It turned out that majority of the patients had relatively stable dose conformity within CTV than PTV as shown in figure 3.3. There were 9 out of 11 patients who had $V95\%_{CTV}$ variation within 3% for all the weekly-CTs. Although patient K showed worst variation up to 13.6% for first weekly-CT and 0.4% variation for last weekly-CT. In figure 3.11 the mean and standard deviation for $V95\%_{CTV}$ has been demonstrated for all the eleven patients. The complete result can be seen in appendix, table A.1 (b).

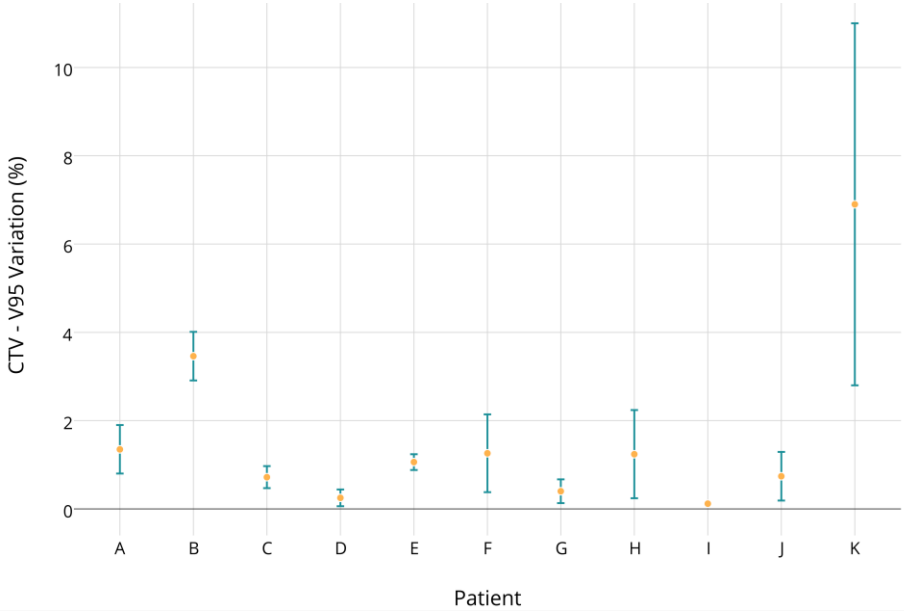

Figure 3.11: Mean and standard deviation of $V95\%_{CTV}$ variation represented individually for all the 11 patients

3.3.2 Gamma-Index

Gamma analysis was performed to compare planning dose distribution with their respective weekly-CTs as shown in figure 3.12. In figure 3.13 the mean and standard deviation for gamma passing rate has been demonstrated for all the eleven patients. The complete result can be seen in appendix, table A.1 (b).

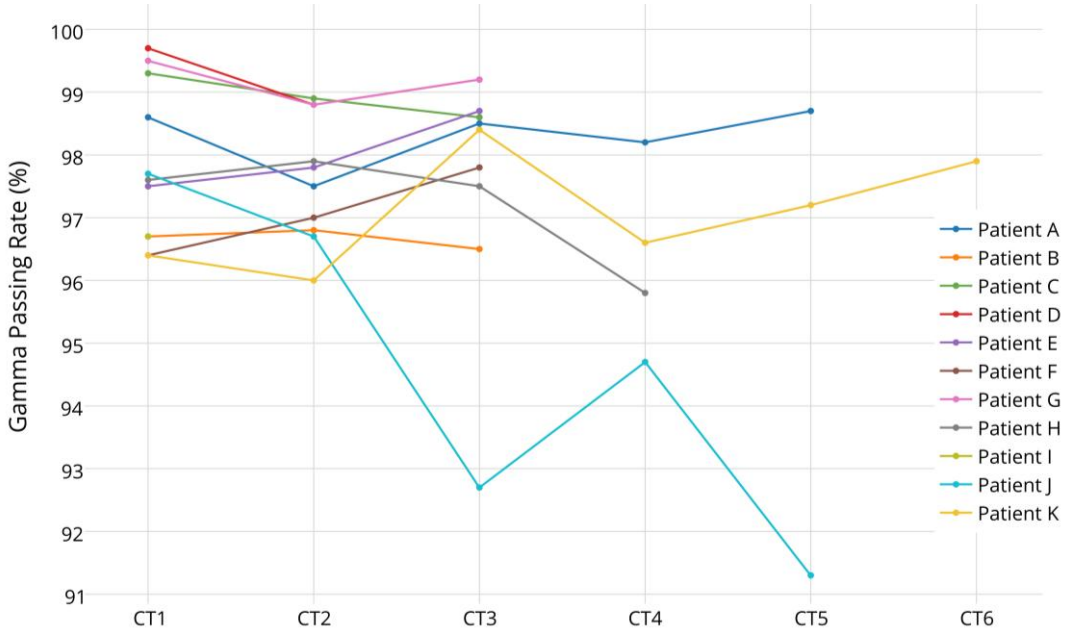

Figure 3.12: Gamma passing rate along the weekly-CTs for all the 11 patients in reference to planning-CT

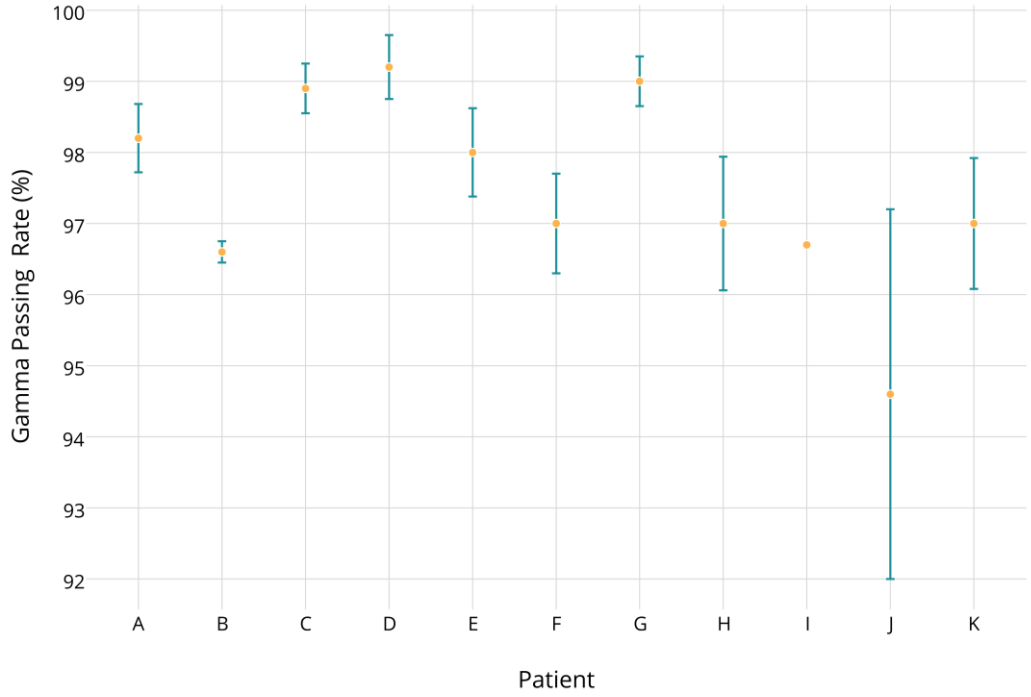

Figure 3.13: Mean and standard deviation of gamma passing rate represented individually for all the 11 patients

There were 5 out of 11 patients who had gamma passing rate of more than 97% for all the weekly-CTs. The lowest passing rate was 91.3% and the highest was 99.7%. We can relate the worst cases to their dosimetric parameters, for example patient J shows major variation of gamma passing rate because this patient had gradual decrease of D_{min} in PTV (shown in figure 3.7) from 1 GyE to almost 0 GyE as the number of weekly-CT increased (see similar trend shown in figure 3.12).

3.3.3 OAR Dose Evaluation

As mentioned in section 3.2.4 this study includes only 3 OARs for dose evaluation (bowel, kidneys and spinal cord). Table 3.3 shows the parameters under evaluation and the results by taking average and standard deviation over all the eleven patients and weekly-CTs. The complete result can be seen in appendix, table A.2.

OAR	**Parameter**	**Plan** (mean and std. dev)	**Weekly-CTs** (mean and std. dev)	**Range**	
				Plan	**Weekly-CTs**
Bowel	V20 (%)	16.3 ± 5.64	16.8 ± 5.64	[9.3; 24.3]	[3; 24.4]
	V80 (%)	7.26 ± 3.77	8.11 ± 4.46	[1.67; 13.7]	[1.14; 17]
Right Kidney	V40 (%)	19.57 ± 10.76	19.7 ± 7.85	[11.1; 46.8]	[7.8; 37.2]
Left Kidney	V40 (%)	19.27 ± 12.56	23.2 ± 11.7	[0; 41.6]	[0; 40.7]
Spinal Cord	Dmax (GyE)	37.2 ± 3.71	37.3 ± 3.71	[32.4; 45.36]	[32.4; 45.36]

Table 3.3: Comparison of dose volume data of the OARs acquired from dose volume histogram (DVH) analyzed for this study. (Average and standard deviation was taken over all the 11 patients and all the weekly-CTs)

Bowel movements have been a major concern in inter-fractional motion for most of the patient in this study. It turned out that the air in bowel along the beam path resulted in over-dosage of the bowel lying distally to the target volume. Figure 3.14 demonstrates variation of the amount of volume receiving 20% of the prescribed dose, for half of the patients it remained consist or slightly lower for the weekly-CTs in comparison to the plan. However figure 3.15 showed high increase in the amount of volume receiving 80% of the prescribed dose, for example patient B the amount of bowel increased gradually from 9% for the CT of the week 1 up to 17% for the week 3.

This concludes that the aforementioned effect of bowel movements result in high dosage to increased amount of volume, although the dose to the target doesn't reflect this variation.

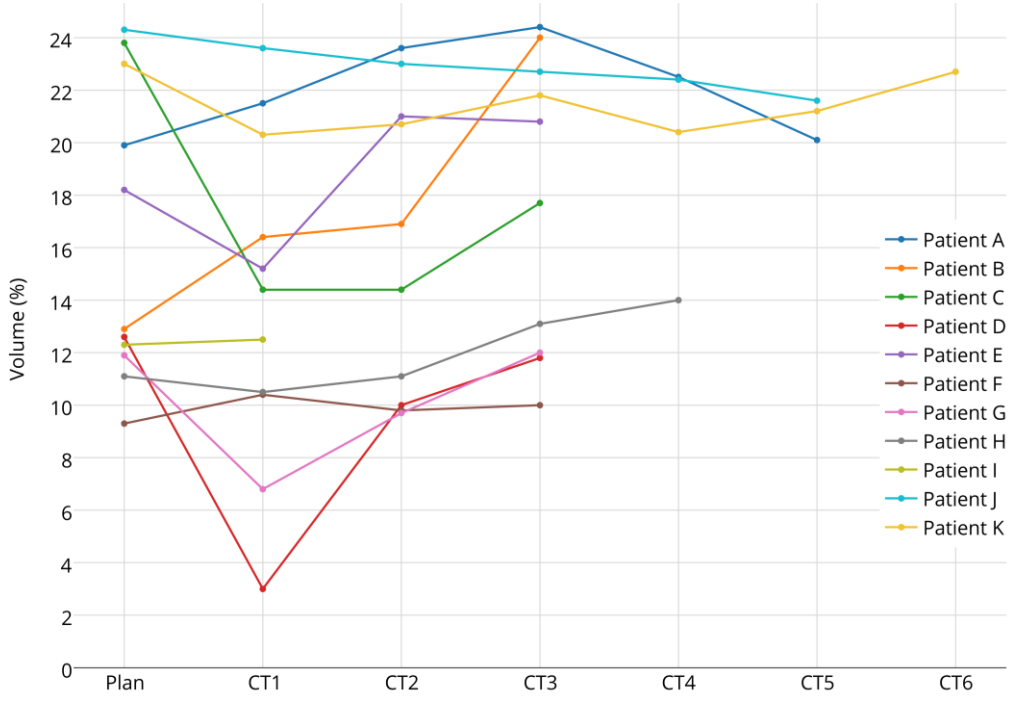

Figure 3.14: Bowel V20 evaluation representing variation along the weekly-CTs in reference to planning-CT for all the 11 patients

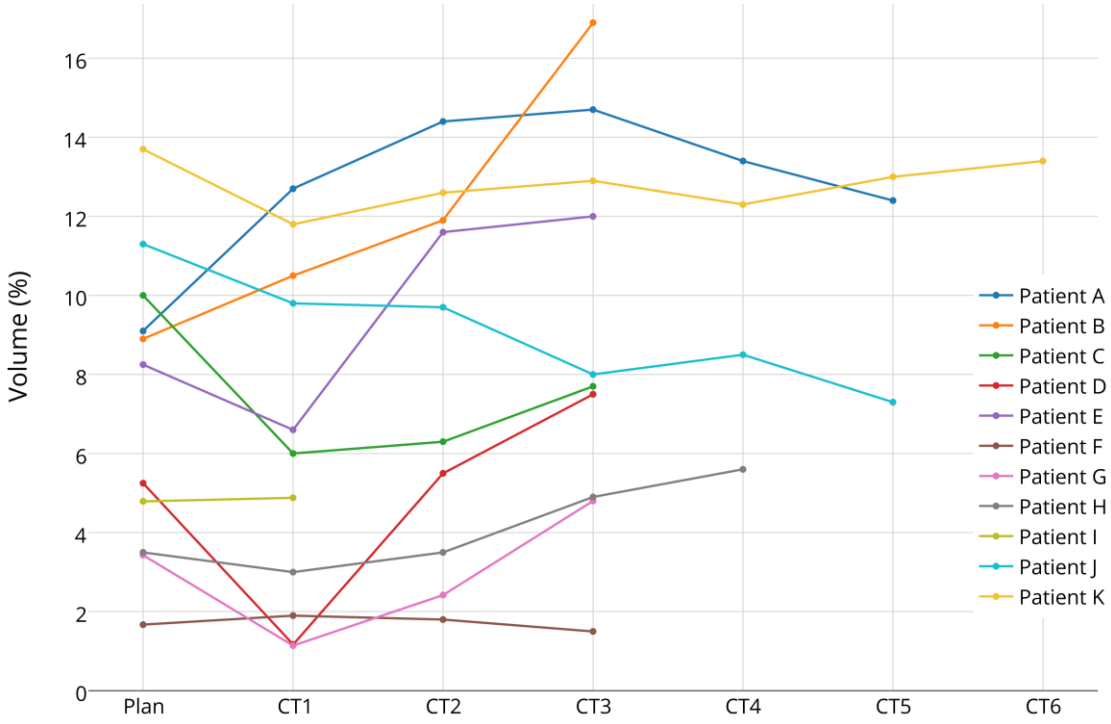

Figure 3.15: Bowel V80 evaluation representing variation along the weekly-CTs in reference to planning-CT for all the 11 patients

As far as kidneys and spinal cord are concerned, inter-fractional motion does not appear to be highly effective on these OARs. The spinal cord D_{max} along the weekly-CTs remained persistent with the planning-CT for the entire set of patients with the exception of patient F whose D_{max} increased by 1%. Similarly, for kidneys, receiving 40% of the dose, remained under (or consistent) with planning-CT for all the eleven patients.

All the result from this chapter can be seen in appendix table A.1 (a), table A.1 (b) and table A.2. Moreover, the absorbed dose distribution images for all the 11 patients can be seen in appendix, figure A.3.

3.4 Summary

The results from this chapter shown that the inter-fractional motion effects the absorbed dose distribution; however the degree of effect depends on the amount of tissue variations caused by inter-fractional motion along the beam path. In terms of target volume the dose conformity for CTV was less affected by the inter-fractional motion in comparison to PTV. It turned out that the air in bowel causes the range uncertainty of the beam resulting in over dosage of the bowel as well.

Chapter 4
WEPL Assessment

4.1 Introduction

This chapter explains a detailed study about water equivalent path length variation (∆WEPL) caused by inter-fractional motion. In the previous chapter the effect of inter-fractional motion on the absorbed dose distribution had been studied and the contributing factors were discussed while this chapter will essentially aid in quantifying the effect of those factors by calculating WEPL. In the following an introduction of the software used has been given for WEPL calculation and its features have been explained. Moreover it explains the detail about the parameters used for evaluation purposes and the types of analysis performed. Lastly, results are presented.

4.2 Method and Materials

For the WEPL analysis the same dataset of patients was utilized as in the plan quality assessment (chapter 3). The analysis was performed on the MeVisLab framework [40], in a module that was developed at the HIT facility, as part of the SPARTA project funded by the *German Research Foundation*. Analysis was done by comparing planning-CT to weekly-CTs. For the stated purpose, all the patient images were rigidly registered in the same manner as it was done for dose forward calculation (section 3.2.3) by implementing the image registration parameters acquired from 3D Slicer into MeVisLab module to depict the same patient alignment. The contoured structures set were transferred to MeVislab from Syngo TPS *(RT planning by Siemens)* for analysis.

4.2.1 MeVisLab- Module Workflow

After the image registration process, the software generates WEPL maps for one treatment field at a single time by defining isocenter (gantry and couch angles) as shown in figure 4.1, considering the HLUT table from the selected CT imaging protocol. Once the field is defined, the volume of interest (VOI) (explained in section 4.4.3) need to be set as a reference target for which the analysis should be performed and also the type of analysis, which will be explained in section 4.2.3. The software generates the accumulated WEPL (accWEPL) in the individual beam's eye view

(BEV), by rotation of the CT according with the given gantry and couch angles. The accWEPL incorporate all the tissue variations for planning-CT and weekly-CT along the beam path for the selected VOI projected in BEV, as shown in figure 4.2. Additionally, the module also generates an accWEPL difference map by subtracting both the individual maps as shown in figure 4.3.

Figure 4.1: MeVisLab interface for defining isocenter, gantry and couch angle

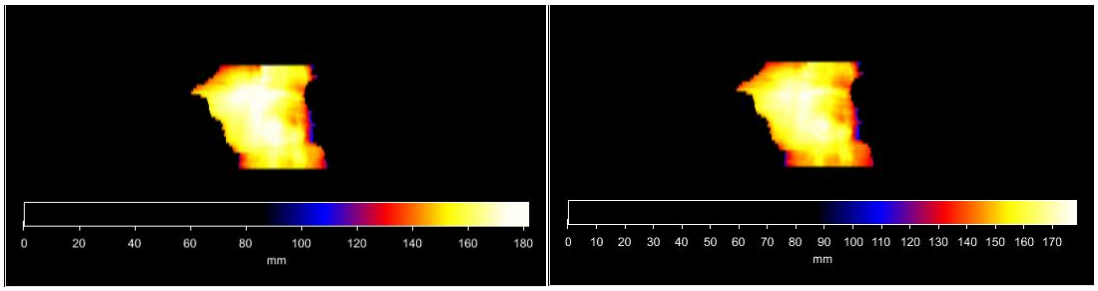

Figure 4.2: Individual BEV showing accWEPL for planning-CT (left) and weekly-CT (right); example of patient E for weekly-CT 1

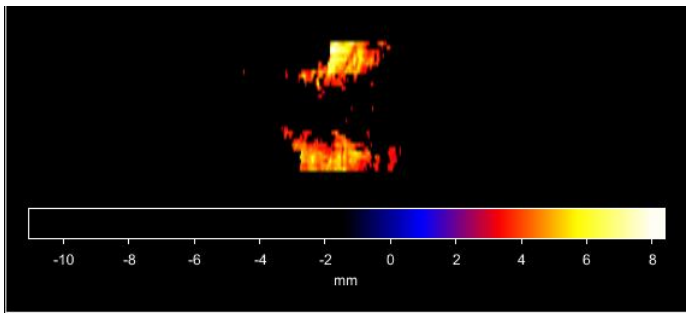

Figure 4. 3: accWEPL difference map of the planning-CT and weekly-CT for the same patient as shown in figure 4.2

4.2.2 Evaluation Features and Tools

For this study, the evaluation was done using the accWEPL difference map of tissue variation among planning-CT and weekly-CT. Most of the time in clinical practice 3 mm-water variation (in absorbed dose distribution) is considered as a general rule, thus for computing accWEPL difference map, a minimum range of tissue variation (in other words, acceptable tissue variations) was set as ±3 mm-water as shown in figure 4.4.

For analysis and visualization purposes accWEPL difference maps were set to show only points outside the range of ±3mm. At this point, the software shows a difference map as in figure 4.3 where different colors represent variations in millimeters as it was set in scalar bar at the bottom of the map, however the black

area within the map represents points within the range of ±3mm. Simultaneously a histogram is generated depicting the number of voxels lying inside and outside the range set as shown in figure 4.5; this histogram gives a percentage of voxels lying inside the defined range and is denoted as PV_{in}. If PV_{in} is higher that means less tissue variations represent more than ±3mm variation and if PV_{in} is low then higher possibility of having tissue variations larger than ±3mm.

Figure 4.4: The range setting option to visualize the accWEPL difference map with only the point which lies outside range set.

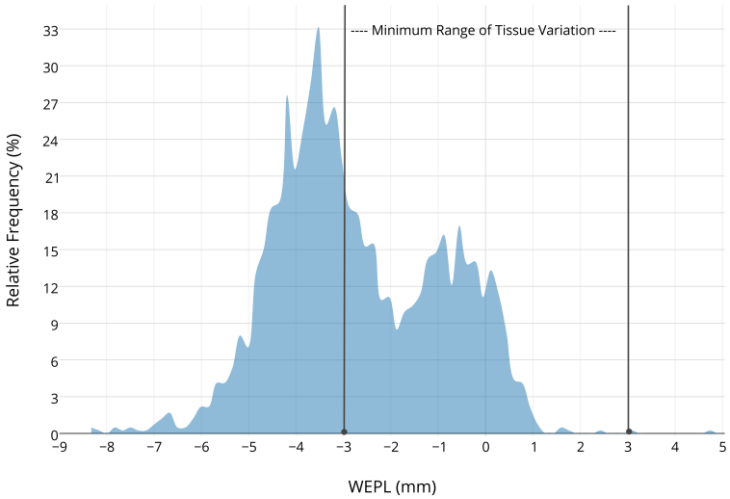

Figure 4.5: Histogram corresponding to accWEPL difference map, showing number of voxels within and outside the range; example of patient J for field 1

Furthermore, the software also gives an option of visualizing per beam experienced variation on the accWEPL maps, which helps in knowing the exact amount of tissue variation in millimeters as ‘current value’ for a specific voxel. Also the variation along the beam path can be seen in CT-value (HU) as a CT profile for that specific beam as shown in figure 4.6, 4.7, 4.8 and 4.9.

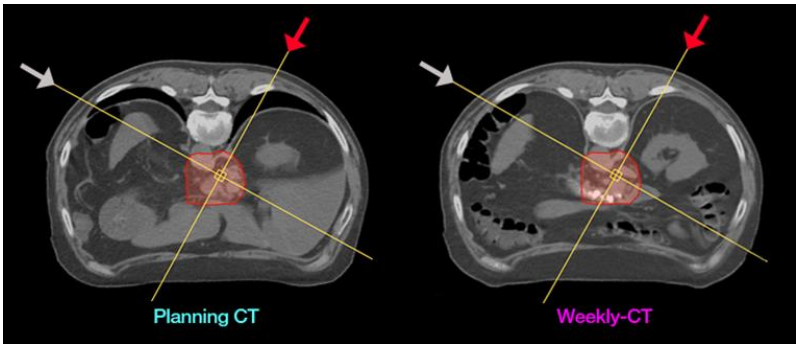

Figure 4.6: Example of patient B showing tissue variation along the beam path for same slice in planning-CT and weekly-CT. (Red arrow= active field direction, grey arrow= inactive field direction during the WEPL calculation)

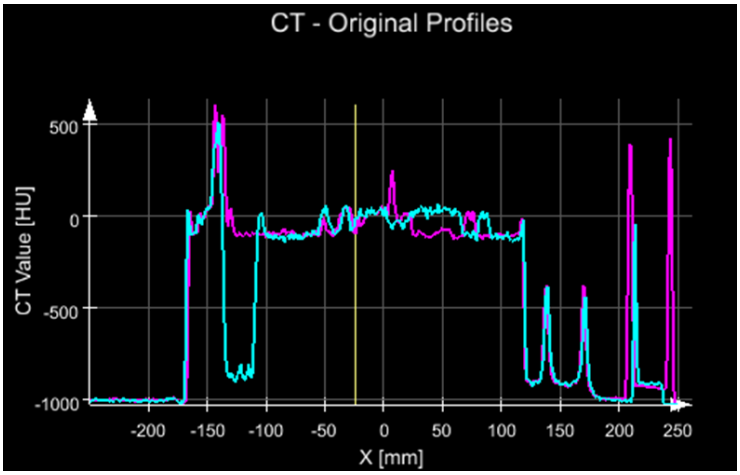

Figure 4.7: Example of patient B; variation of density given by the CT-value along the same beam path as shown in figure4.6 (Aqua blue=planning CT, magenta= weekly CT)

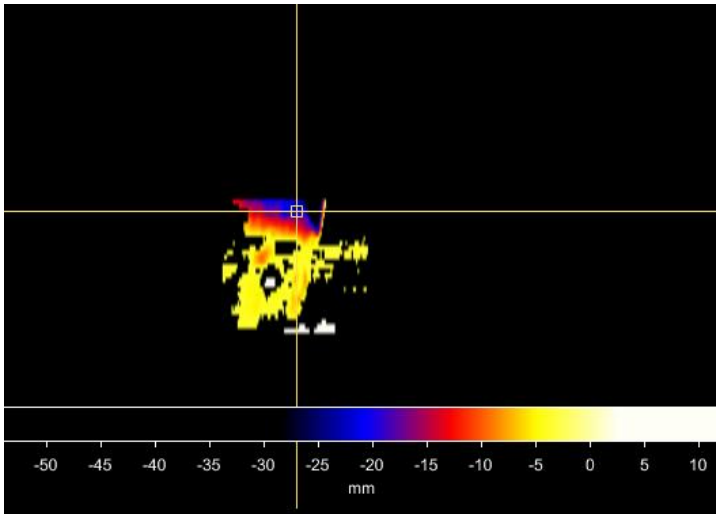

Figure 4.8: Example of patient B; same point indication on accWEPL difference map as shown in figure 4.6 and 4.7

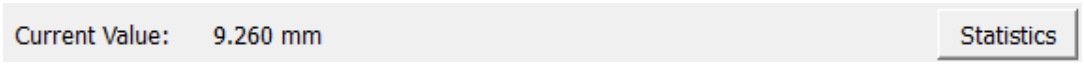

Figure 4. 9: Showing the current value from accWEPL map for the specific point shown in figure 4.8

4.2.3 Evaluation Parameter

Volume of interest (VOI)

From the contoured structure set, CTV was selected as a reference volume, additionally a margin of 1mm in x, y directions (anterior-posterior and left-right) and 3mm in (superior-inferior) z direction was introduced as shown in figure 4.10. This entire volume including CTV and the margins was denoted as volume of interest (VOI). Although, above mentioned margins does not have any clinical or dosimetric relevance.

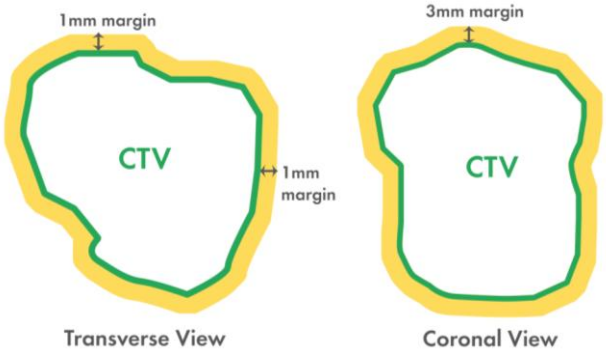

Figure 4.10: Illustration of volume of interest used for WEPL map generation

Normalized PV_{in} (PV_{norm})

As explained in section 4.2.1, MeVisLab module computes a PV_{in} value per field from the accWEPL difference maps. Since the patients in this study had at least 2 fields and at most 3 fields (refer to table 3.1) the PV_{in} of each field was normalized by taking into account the respective field weight. This was done by averaging the field intensity i.e. number of particles (information acquired from raster scanning data of the initial treatment plan) from both fields. The resultant intensity was multiplied with PV_{in} for each field, summed up and divided by the total number of particles of the complete plan. The end result was denoted as normalized PV_{in} (PV_{norm}) which was calculated for each weekly-CT of all the patients.

4.2.4 Types of Analysis

To evaluate the tissue variation along the beam path, two analyses were performed for the VOI to generate accWEPL difference maps as shown in the figure 4.11.

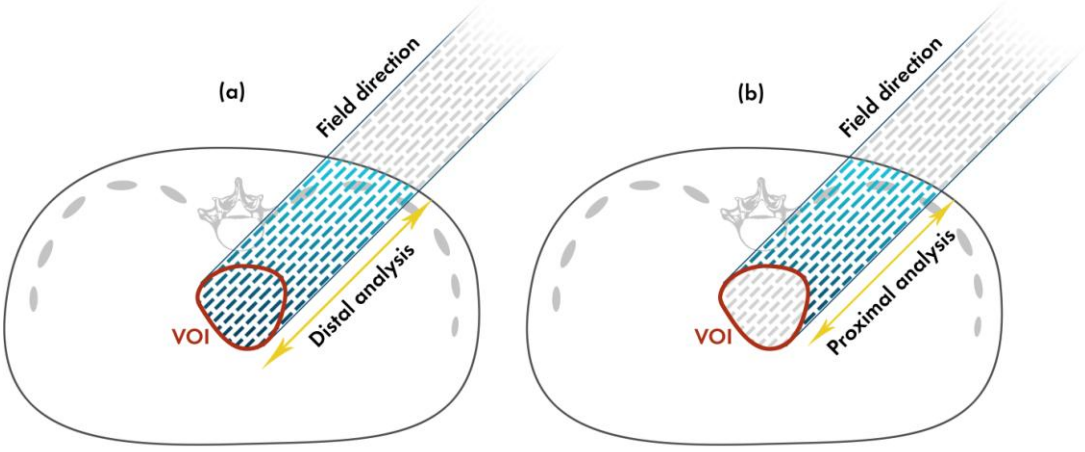

Figure 4. 11: Illustration of types of analysis option used for calculating accWEPL. (a) Distal analysis, (b) Proximal analysis

Distal edge analysis: In this method, the WEPL is summed up along the beam path, starting from patient skin to the distal edge of the VOI in the BEV direction, see figure 4.11 (a).

Proximal edge analysis: In this method, the WEPL is summed up along the beam path, starting from patient skin to the proximal edge of the VOI in the BEV direction, see figure 4.11 (b).

4.3 Results – WEPL maps

4.3.1 Distal Analysis

The results from distal analysis for all the eleven patients along the weekly-CTs are demonstrated in figure 4.12. For 6 out of 11 patients who had better PV_{norm} (around 70% and above) for first weekly-CT, the PV_{norm} tend to decrease by 10% to 23% for the second weekly-CT (Patients B,C,D,E,G,K). Only two patients demonstrated consistent behavior by having PV_{norm} within 3% along the weekly-CTs (Patient F, H). For patient J, large variations of up to 42% observed from weekly-CT2 to CT5. In figure 4.13 the mean and standard deviation of PV_{norm} for distal analysis are demonstrated for all the eleven patients. The complete result of distal analysis can be seen in appendix, table A.1 (b).

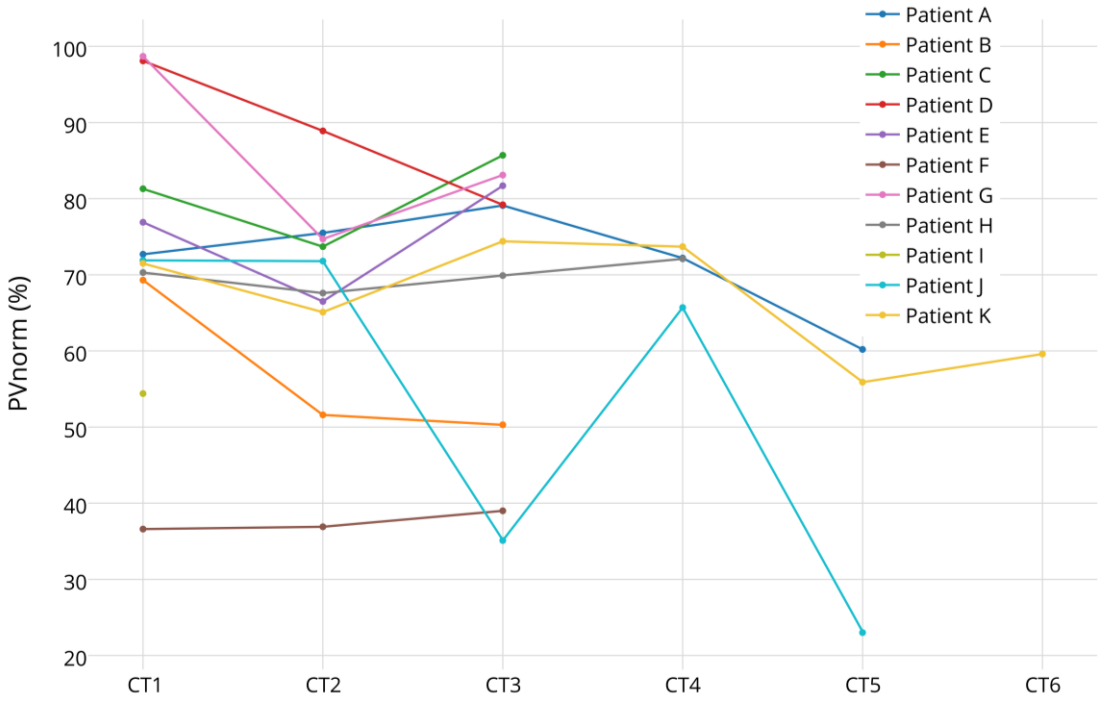

Figure 4.12: PV_{norm} variation from distal analysis along the weekly-CTs of all the 11 patients

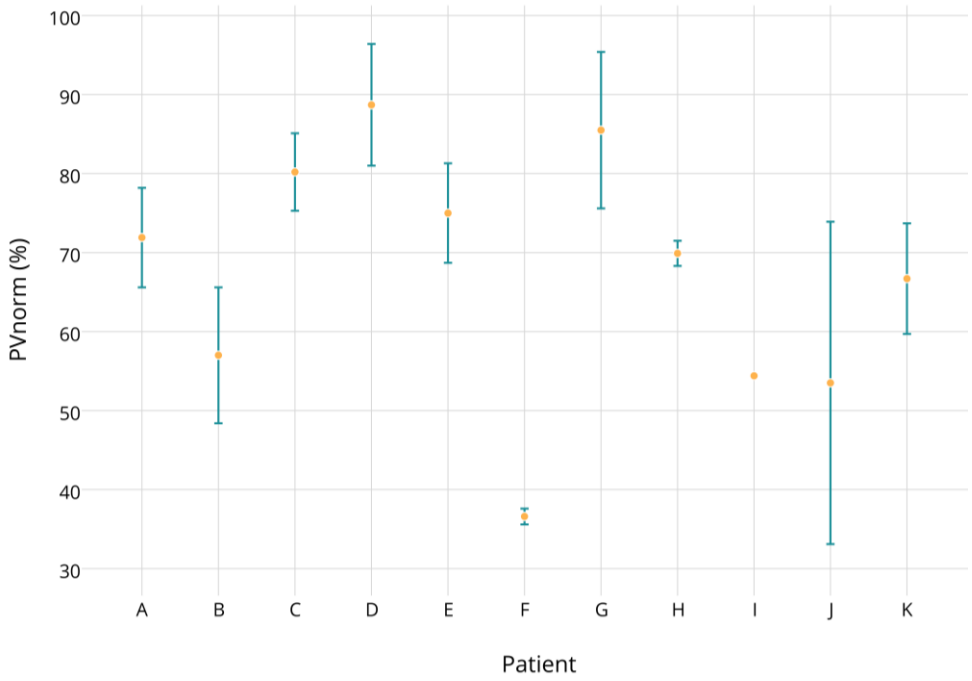

Figure 4.13: Mean and standard deviation of PV_{norm} for distal analysis

4.3.2 Proximal Analysis

The results from proximal analysis for all the eleven patients are shown in the figure 4.14. The complete result of proximal analysis can be seen in appendix, table A.1 (b).

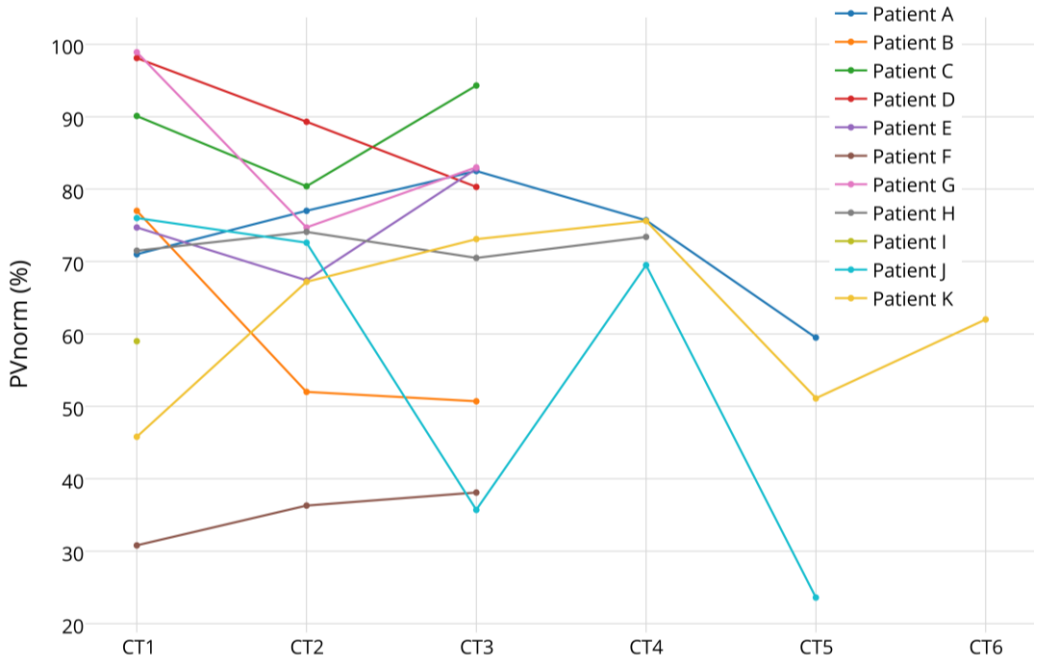

Figure 4.14: PV_{norm} variation from proximal analysis along the weekly-CTs of all the patients

Those 6 patients mentioned in distal analysis showed same pattern of decrement in PV_{norm} after the first weekly-CT. Patient F had a consistent behavior in distal analysis with PV_{norm} within 3% which changed to 6% in proximal analysis. For patient J and K, the variations became more prominent in comparison with distal analysis. In figure 4.15 the mean and standard deviation of PV_{norm} for proximal analysis are demonstrated for all the eleven patients.

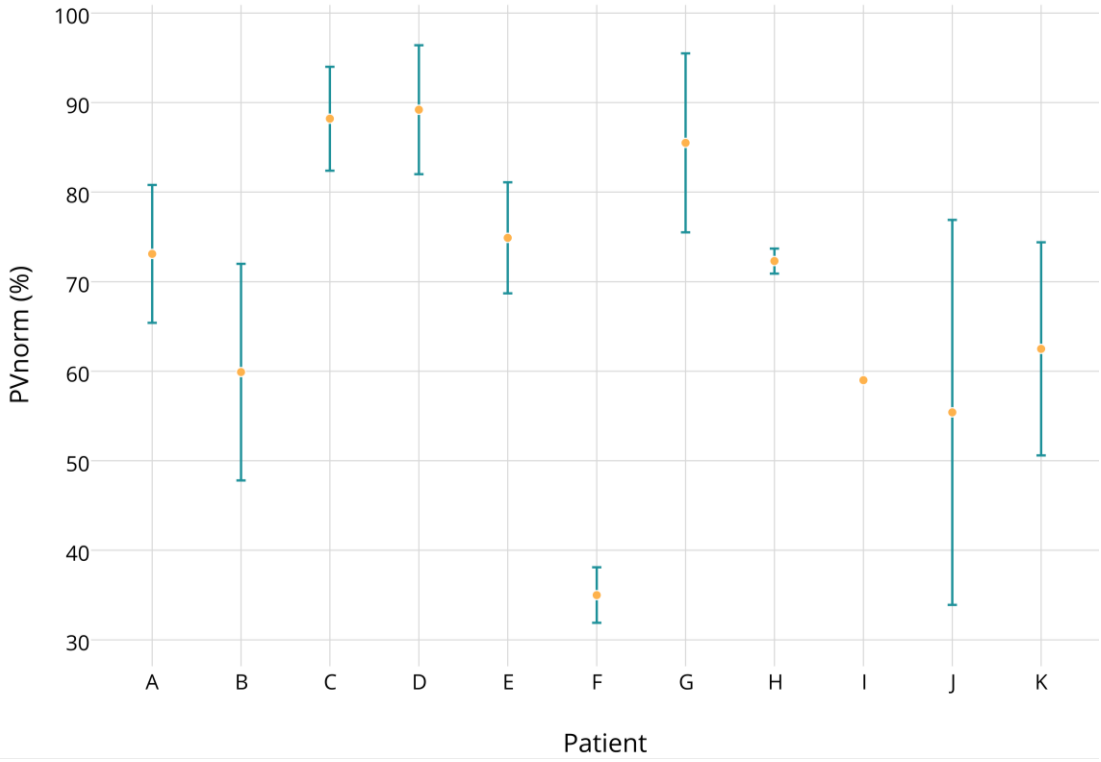

Figure 4.15: Mean and standard deviation of PV_{norm} for proximal analysis

4.3.3 Comparison of Proximal and Distal Analysis

As mentioned in section 4.2.3 the variation in accWEPL was assessed till the distal and proximal edge of the VOI, the comparison among distal and proximal analysis could actually depict that where majority of the density variation experienced by WEPL. For this purpose the total number of weekly-CTs from all the eleven patients, which makes 39 sets (see table 3.1) were considered as points separately for both distal and proximal analysis as shown in figure 4.16.

It turned out that 26 out of 39 points were within 3% for both distal and proximal analysis which means variations in proximal analysis has 66% same amount of variations as in distal analysis. This results emphasis on the fact that in the majority of the cases increased density variation occurs outside the VOI and the target density changes are almost neglected.

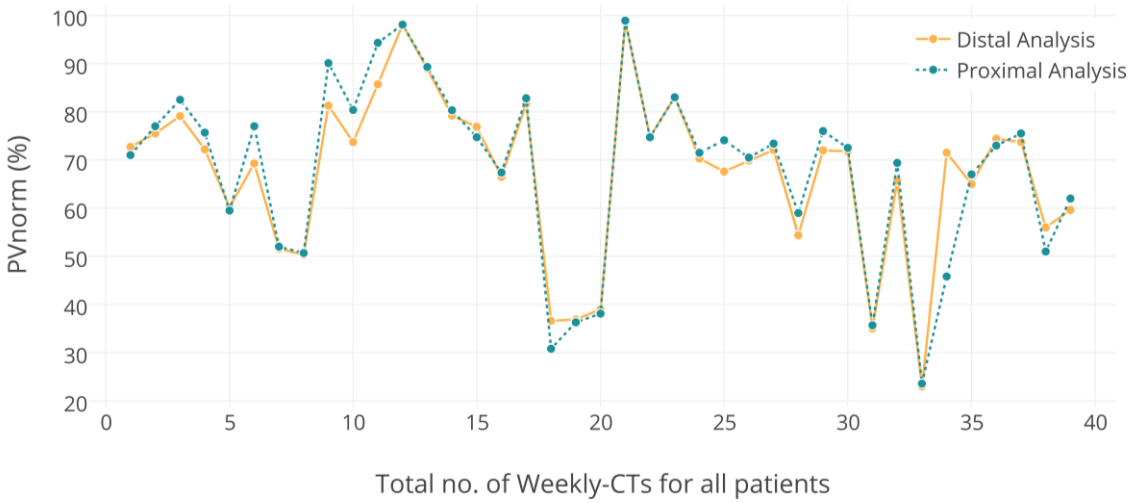

Figure 4.16: Comparison of proximal and distal analysis; showing PV_{norm} variations for all the weekly-CTs included in this work

4.4 Summary

In this chapter the rationale was to quantify the effect of inter-fractional motion on WEPL. For this purpose a parameter was defined to evaluate the WEPL variations for each field and depict the combined effect. It turned out that the major variation in WEPL was primarily effected by the bowel movements (even with prone position) as we already concluded in Chapter 3. Secondly, WEPL variations were also affected by the change in amount of lung within the treatment field on daily basis and also due to the positioning error. The aforementioned effect was making major difference outside VOI, however, within VOI had slight effect.

Chapter 5

WEPL Correlation & Criteria Definition

5.1 Introduction

In the previous chapter the goal was to quantify the density variation caused by inter-fractional motion by using WEPL. Also we have already discussed in chapter 3 the effected dose distribution parameters. In this chapter, the correlation among dosimetric parameters and PV_{norm} calculated from accWEPL difference maps (which were evaluated in chapter 3 and chapter 4 respectively) has been observed. This was done by considering the dosimetric and WEPL variations on each weekly-CT from all the eleven patients. The goal was to find the best dosimetric parameter, which would strongly correlate with WEPL variation in a situation of high density variations. Furthermore, it was also the aim to obtain the criteria of WEPL variation which would help in predicting the resultant dosimetric effects on the dose distribution.

5.2 Method and Materials

This section explains about the parameters and method used to establish a dosimetric correlation, also describes the method for defining the threshold criteria.

5.2.1 Correlation Parameters

To evaluate the correlation among WEPL and dosimetric parameter, which were discussed in chapter 3 and 4, PV_{norm} was correlated with the variation of $V95\%_{CTV}$, variation of $V95\%_{PTV}$, gamma passing rate and for the most meaningful OARs doses (i.e, bowel).

5.2.2 Correlation Method

The Pearson correlation coefficient (denoted by *r*) was used to measure the strength of linear association among WEPL and dosimetric parameters. Additionally, a linear regression with the attempt to define the best linear fit is performed (straight line), which will help in showing how far the data points are from a linear fit. Also 95% confidence band has been drawn along the straight line.

5.2.3 Parameter Selection for Criteria Definition

For the definition of the accWEPL variation criteria, those dosimetric parameters were considered which were moderately or strongly correlated with PV_{norm}.

5.2.4 Action and Tolerance level definition

By considering clinically reasonable variation in V95% and gamma passing rate, action and tolerance level were defined. For the variation in V95%, either for CTV or PTV, 2% and 3% variation was set as tolerance and action level respectively. Similarly, for gamma passing rate 97.5% and 96.5% were considered as tolerance and action level respectively. These values were used to compute the corresponding PV_{norm} by using the straight line equation from the correlation plots.

5.3 Results

5.3.1 CTV – V95%

The correlation of $V95\%_{CTV}$ variation and PV_{norm} of distal analysis has been demonstrated in figure 5.1.

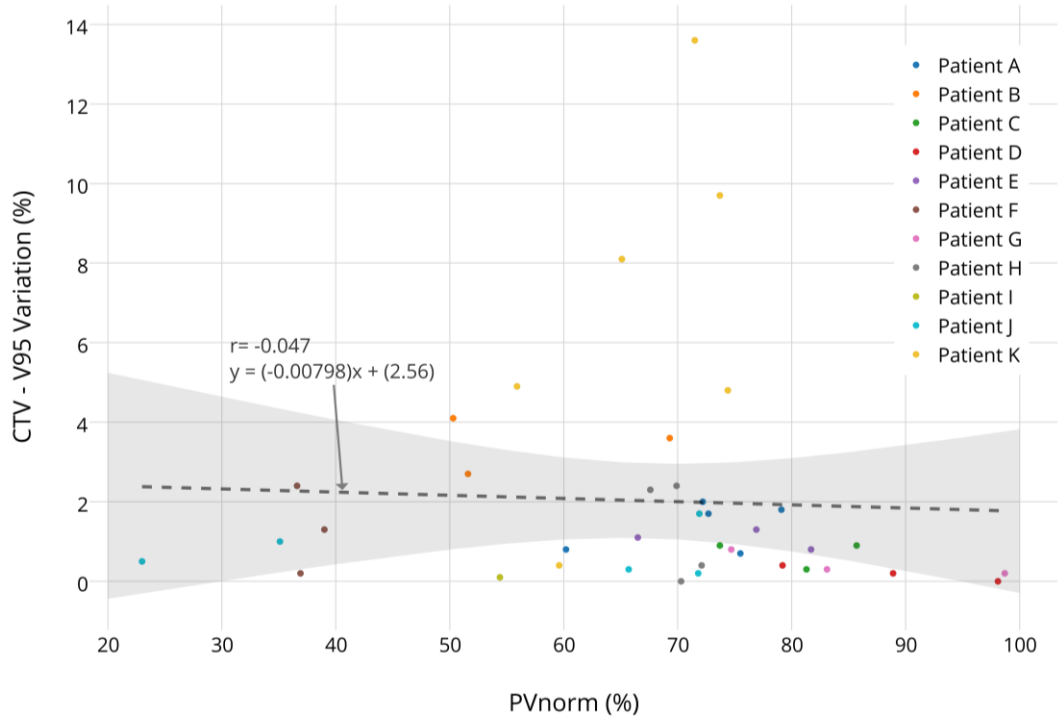

Figure 5.1: The correlation of $V95\%_{CTV}$ variation and PV_{norm} for distal analysis, for all the 11 patients; where r=Pearson correlation coefficient, grey dashed line = linear regression (calculated from straight line equation shown as y), grey band= 95% confidence band

It was found that $V95\%_{CTV}$ variation was not correlated, i.e. r of 0.047, with PV_{norm} and this was an expected result because if we observe the pattern of $V95\%_{CTV}$ variations for all the patients in figure 3.10 and 3.11, there was only one patient who had high variation up to 13.6% and the majority of the patients remained within 3% along the weekly-CTs.

. The correlation of $V95\%_{CTV}$ variation and PV_{norm} for proximal analysis has been demonstrated in figure 5.2. There was a weak correlation among $V95\%_{CTV}$ variation and PV_{norm} but slightly higher correlation, i.e. r of -0.21, in comparison to distal analysis.

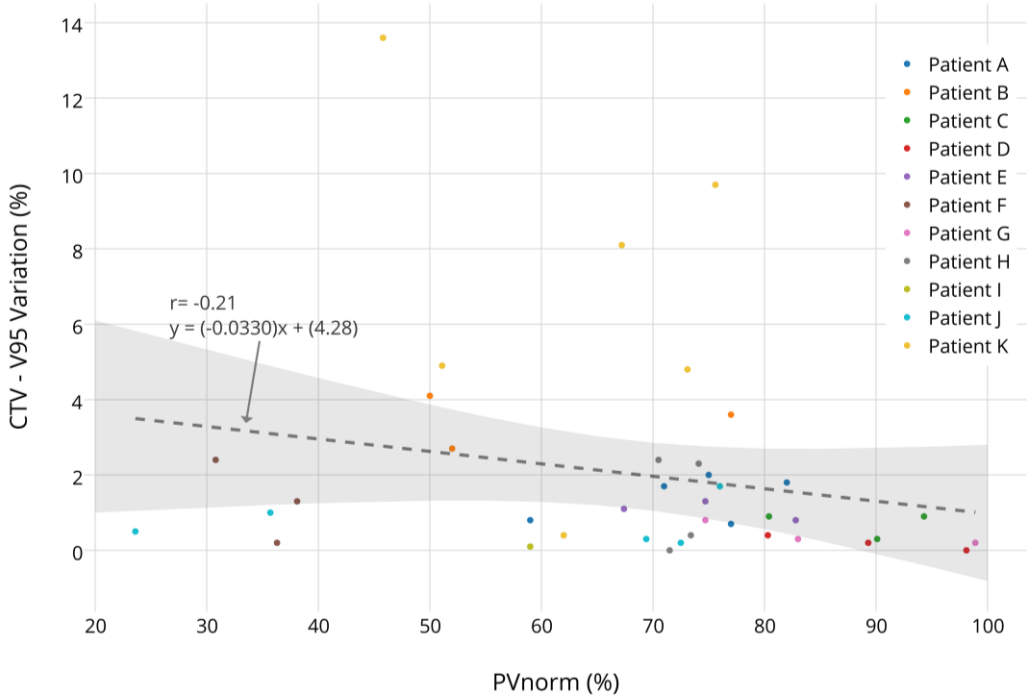

Figure 5.2: The correlation of $V95\%_{CTV}$ variation and PV_{norm} for proximal analysis, for all the 11 patients; where r= Pearson correlation coefficient, grey dashed line = linear regression (calculated from straight line equation shown as y), grey band= 95% confidence band

The combine assessment of distal and proximal analysis explained the reason for having a better correlation for proximal analysis than distal analysis, most of the time CTV remained homogenous with respect to density variation which justified the result in term of proximal vs. distal tissue variations in section 4.3.3. It was also observed that the high density variation within CTV was mainly due to the presence of a surgical clip which is also mobile due to internal organ motion; this fact will be explained further in the discussion section.

5.3.2 PTV - V95%

The correlation of $V95\%_{PTV}$ variation and PV_{norm} of distal and proximal analysis has been demonstrated in figure 5.3 and 5.4 respectively.

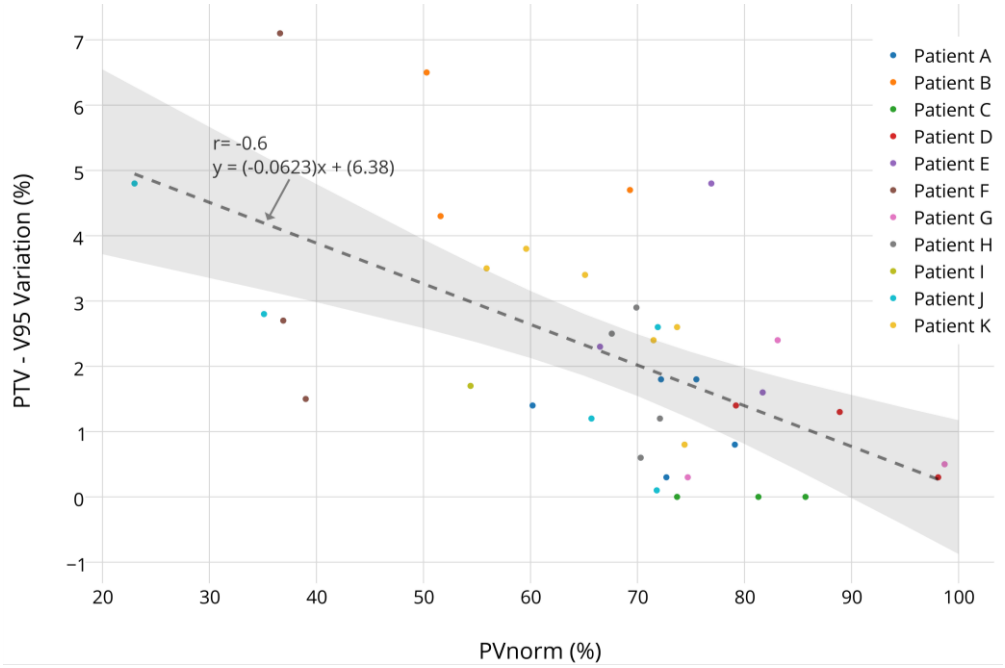

Figure 5.3: The correlation of $V95\%_{PTV}$ variation and PV_{norm} for distal analysis, for all the 11 patients; where r=Pearson correlation coefficient, grey dashed line = linear regression (calculated from straight line equation shown as y), grey band= 95% confidence band

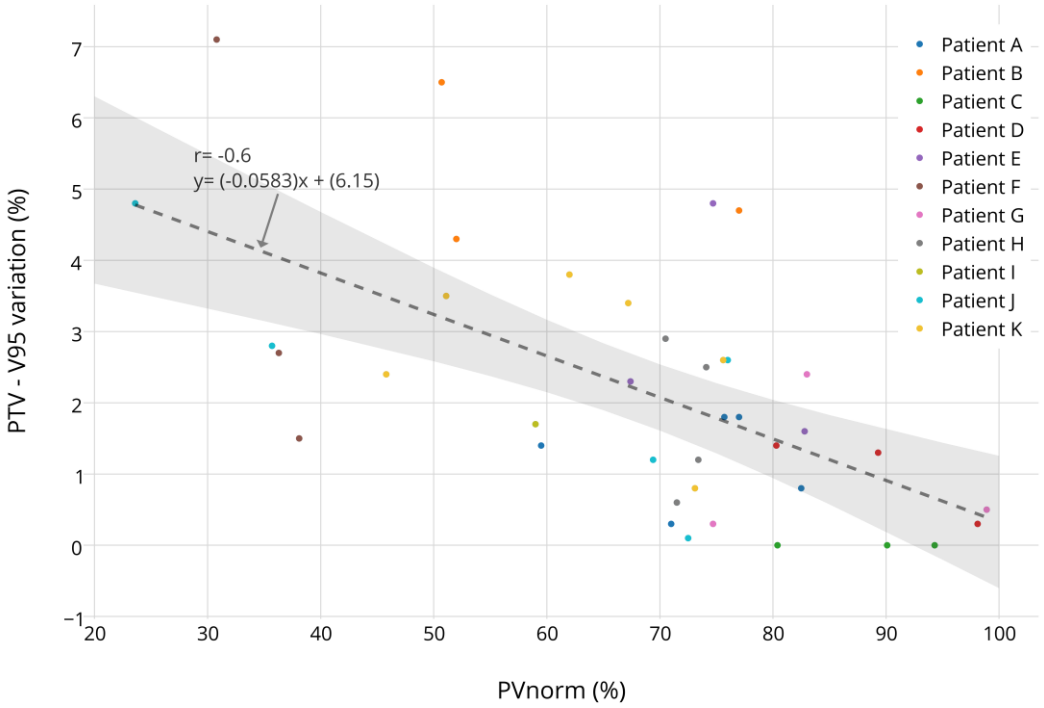

Figure 5.4: The correlation of $V95\%_{PTV}$ variation and PV_{norm} for proximal analysis, for all the 11 patients; where r= Pearson correlation coefficient, grey dashed line = linear regression (calculated from straight line equation shown as y), grey band= 95% confidence band

In both the analyses, $V95\%_{PTV}$ variation and PV_{norm} were strongly correlated with r of -0.6 due to the reason of having high variation in $V95\%_{PTV}$ along the weekly-CTs for majority of the patients as shown in figure 3.3 and 3.4. The reason for having better correlation of PV_{norm} with $V95\%_{PTV}$ than $V95\%_{CTV}$ is that PTV includes the margins of inter-fractional uncertainties thus PTV is more heterogeneous than CTV which results in inhomogeneous dose distribution. Although there were some outliers present which represented higher PV_{norm} also had high variation of $V95\%_{PTV}$.

5.3.3 Gamma Passing Rate

The correlation of gamma passing rate and PV_{norm} of distal and proximal analysis has been demonstrated in figure 5.5 and 5.6.

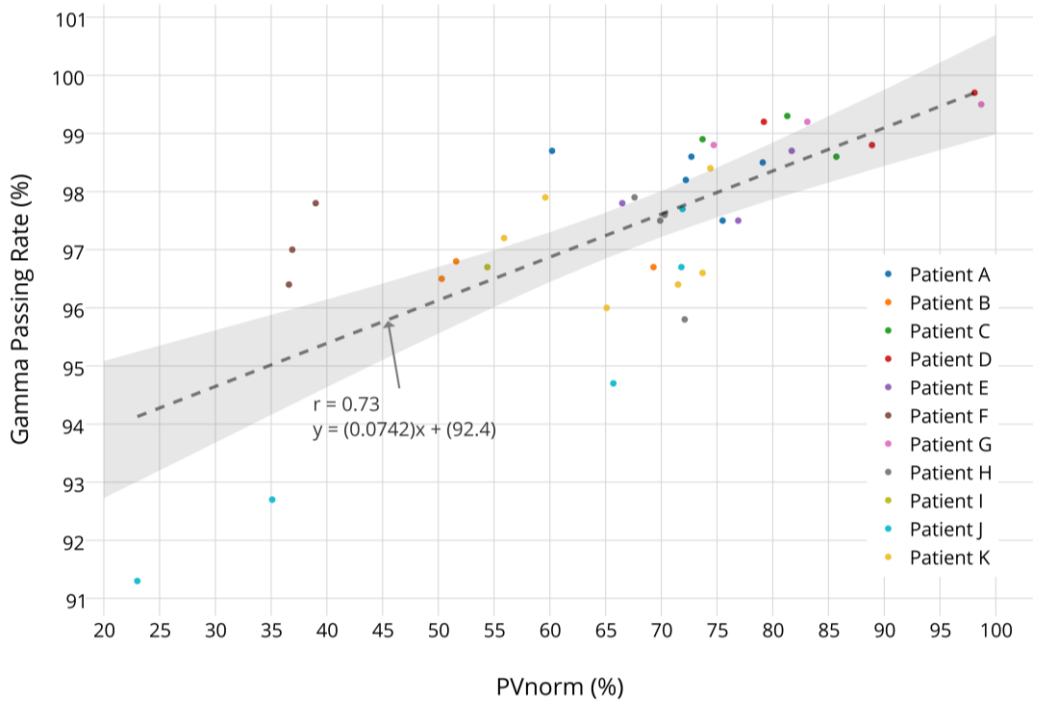

Figure 5.5: The correlation of gamma passing rate and PV_{norm} for distal analysis, for all the 11 patients; where r=Pearson correlation coefficient, grey dashed line = linear regression (calculated from straight line equation shown as y), grey band= 95% confidence band

A very strong correlation, i.e. r of 0.73 for distal and r of 0.7 for proximal analysis, has been observed among gamma passing rate and PV_{norm} since the variation in gamma passing rate fluctuated along the weekly-CTs for all the eleven patients as shown in figure 3.12 and 3.13. The reason for such strong correlation is that gamma index evaluates dose distributions of the absorbed dose plans irrespective of target volumes, which make it sensitive to high or low dose gradients, similarly accWEPL assess density variation along the beam path irrespective of target volume. The number of false positives (high PV norm but low gamma) and false

negatives (low PV norm but high gamma) has reduced in comparison to $V95\%_{PTV}$ correlation because gamma index gives complete information of dose distribution (not only for PTV or CTV).

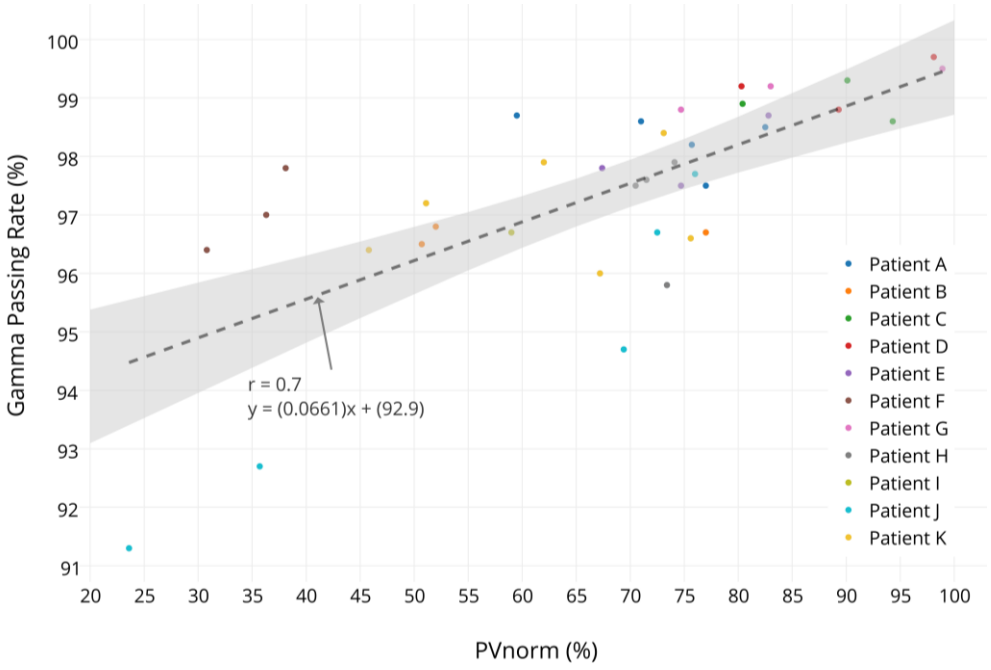

Figure 5.6: The correlation of gamma passing rate and PV_{norm} for proximal analysis, for all the 11 patients; where r = Pearson correlation coefficient, grey dashed line = line of best fit (calculated from straight line equation shown as y), grey band= 95% confidence band

Since the dose distributions variation occurs more outside the target (that means in the normal tissues and OARs) than in the target volumes, this effect can be understood by an example as shown in figure 5.7 where a moderate correlation, i.e. r of -3.8, has been found among $V20_{bowel}$ and gamma passing rate. This also depicts that higher gamma passing rate give lower $V20_{bowel}$ and vice versa.

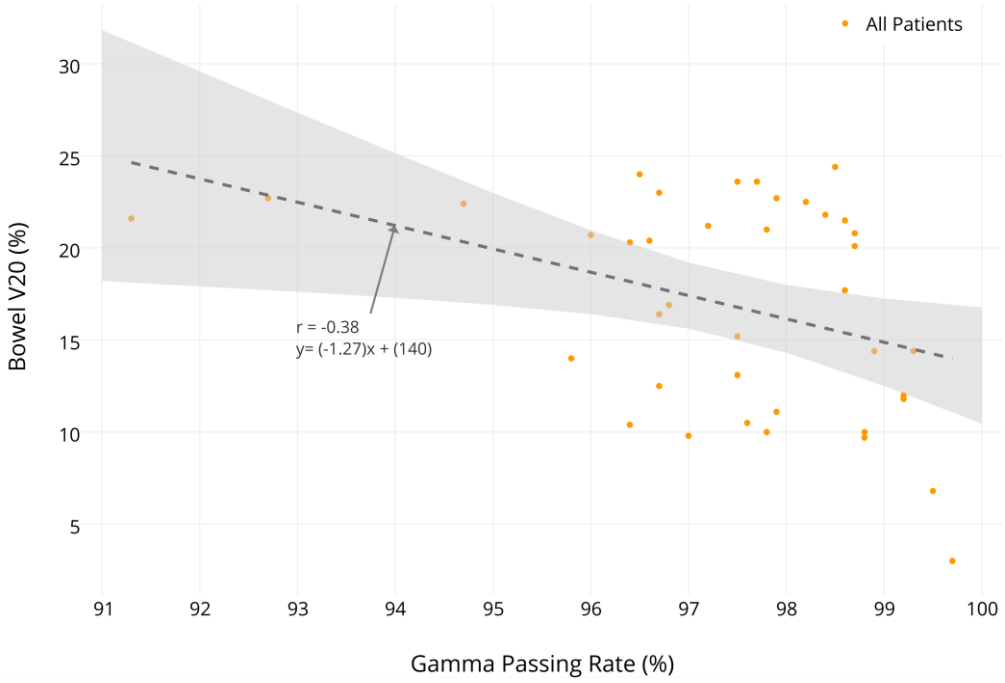

Figure 5.7: The correlation of Bowel V20 with gamma passing rate for all the 11 patients; where r = Pearson correlation coefficient, grey dashed line = line of best fit (calculated from straight line equation shown y), grey band= 95% confidence band

5.4 Decision Criteria Definition (PV_{norm} Threshold)

The assessment, evaluation and correlation of dosimetric parameters brought this study to a conclusive stage where a criterion of PV_{norm} can be predicted which could suggest the onward effects of dose distribution due to tissue variations. As explained in section 5.3.2 and 5.3.3 that both Gamma-index and $V95\%_{PTV}$ showed tendency to increase or decrease with PV_{norm} by strong correlation of 0.73 and 0.6 respectively.

In a real clinical situation we cannot define a strict borderline for prediction that is why a general rule has been defined as a tolerance and action level demonstrated in table 5.1. The rationale of predicting such criteria is to use it as reference guide routinely in clinical patient scenarios; when patients has been imaged before the treatment delivery, a physicist would take 5 to 10 minutes for the calculation of WEPL maps and a physician will evaluate the resulting PV_{norm} to suggest if the patient should be treated or not. Conclusively it will help in plan adaptation.

The tolerance level suggests that below PV_{norm} 70% there is a need to investigate further so as to be sure if patient should be treated or not, however, action level (obtained as a PV_{norm} of 56%) would strongly emphasis on plan re-optimization. One should realize that these defined criteria were defined for the specifications of this

study, i.e., beam geometries, PTV and CTV margins, clinical protocol (that affects the GTV size) and dosimetric acceptance levels.

Criteria	PV_{norm} (%)	$V95\%_{PTV}$ Variation (%)	Gamma passing rate (%)
Tolerance Level	70	2	97.5
Action Level	56	3	96.5

Table 5.1: The criteria definition of PV_{norm} in terms of dosimetric action and tolerance levels

5.4.1 Patient Examples

In the following, patient examples have been explained which supports above mentioned criteria.

1- Patient J

The absorbed dose distribution for planning-CT has been shown in figure 5.8 which represents a worst case in terms of target volume coverage to reduce higher doses to OARs; one can observe the amount of bowel close to CTV and inside PTV. The field configuration, dose per fraction and other specifications for this patient can be seen in table 3.1.

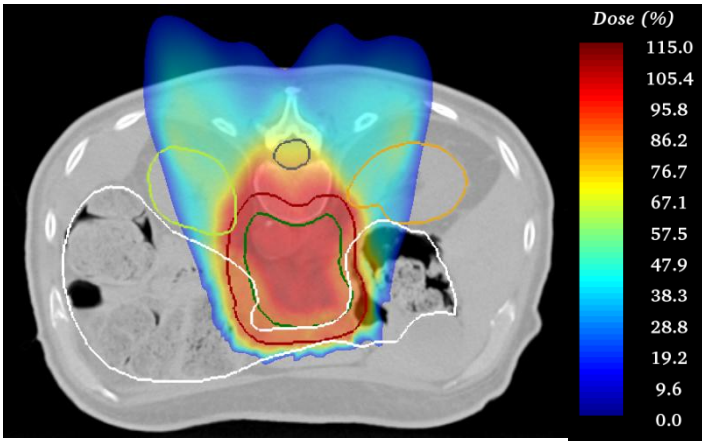

Figure 5.8: Dose distribution of a planning-CT for Patient J. (Contoured OARs and target volumes: grey = spinal cord, lime = left kidney, mustard = right kidney, white = bowel, green = CTV, red = PTV)

The dose volume histogram (DVH) of CTV in figure 5.9 has shown the variations along the weekly-CTs from planning-CT. The $V95\%_{CTV}$ (where 95% dose is 1.7GyE) of planning-CT was 56.4% and the maximum variation for the weekly-CTs was about 1.7% as we have already seen in figure 3.10 and 3.11 less variation for

$V95\%_{CTV}$ along the weekly-CTs. Similarly, $V95\%_{PTV}$ of the planning-CT was 49.5% and the maximum variation was up to 5% for the weekly-CTs as shown in figure 5.10.

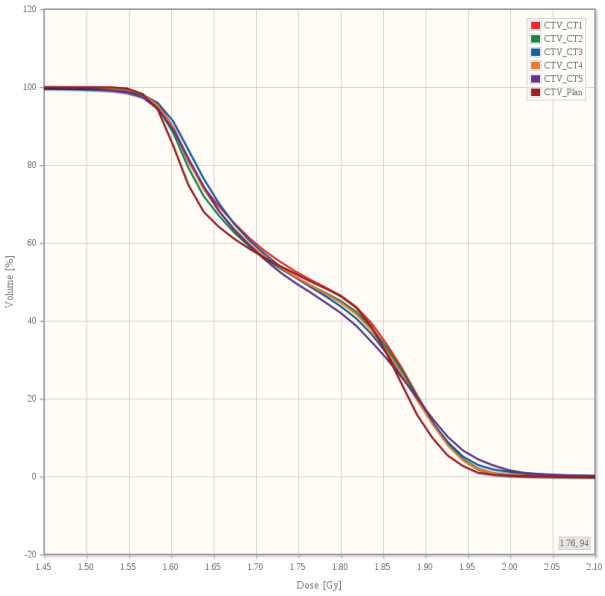

Figure 5.9: DVH of the CTV for the patient J including the evaluation of the planning-CT and 5 weekly-CTs dose distributions; 95% of the prescription dose is 1.7GyE.

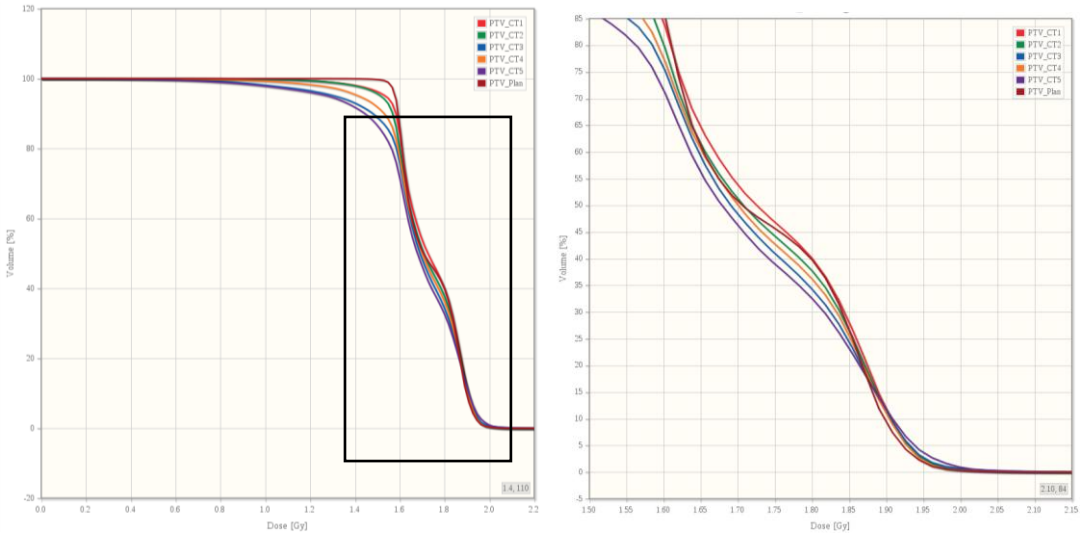

Figure 5.10: DVH of PTV for patient J including planning-CT and 5 weekly-CTs; 95% dose=1.7GyE. (On the left is whole view and on the right is zoomed view)

Figure 5.11 demonstrated that this patient attains the lowest PV_{norm} for weekly-CT3 and CT5 which also correspond to lowest gamma passing rate as well as maximum PTV V95% variation. The reason for having low gamma passing rate was that the minimum dose within PTV reached gradually from 1GyE to almost zero along the weekly-CTs as shown in figure 3.7 although maximum dose stayed consistent as shown in figure 3.5. On the other hand, the minimum dose of weekly-CT4 was equal

to weekly-CT3 which gives a low gamma passing rate but demonstrated $V95\%_{PTV}$ variation close to 1%.

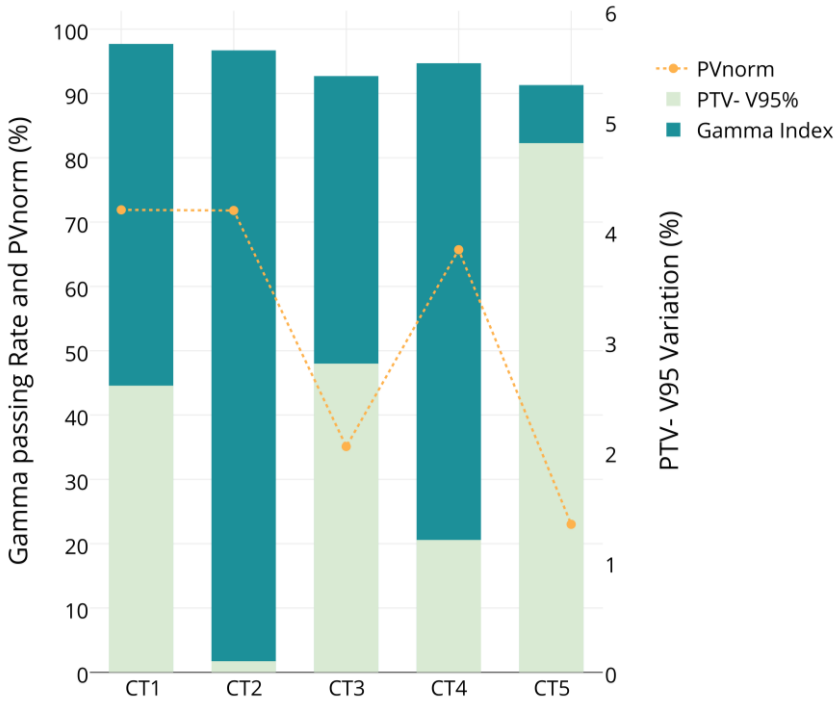

Figure 5.11: Bar graph for Patient J; lower PV_{norm} corresponds to lowest gamma passing rate and high variation in V95% PTV variation e.g. weekly-CT3 and CT5

For detailed analysis of the above mentioned effects, each field was assessed for accWEPL difference to the planning-CT and found that for weekly-CT4 and CT5 the peaks laid outside our defined minimum range ±3mm for tissue variation in both treatment fields as shown in figure 5.12 and 5.13. Also the maximum variation experienced by highest number of voxels was between -6mm to -9mm.

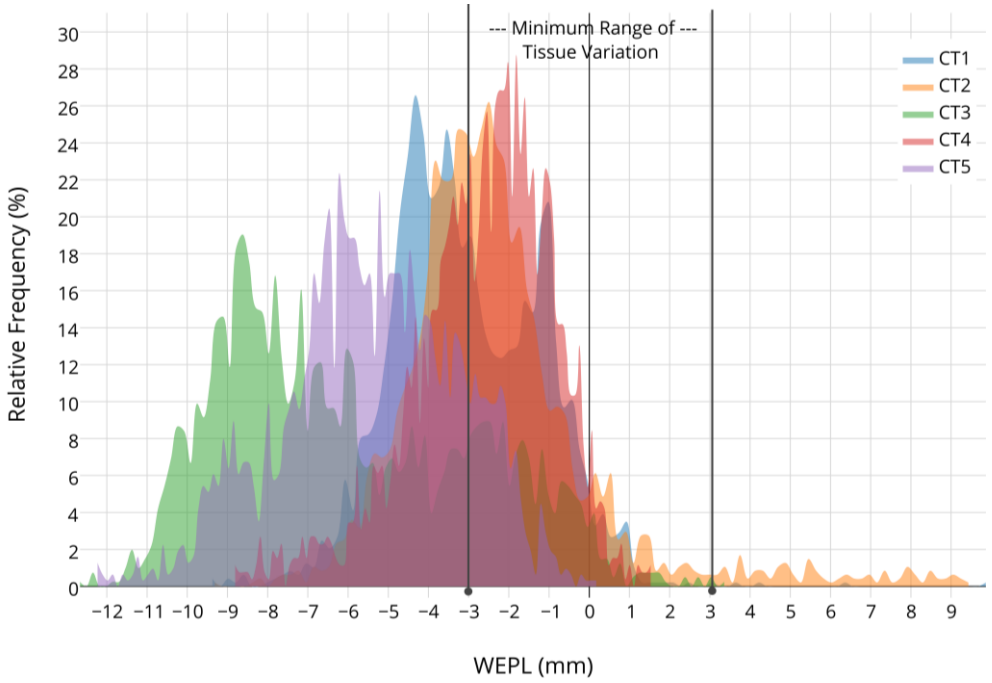

Figure 5.12: Histogram of accWEPL difference map for the Field 1; all the CTs of the Patient J.

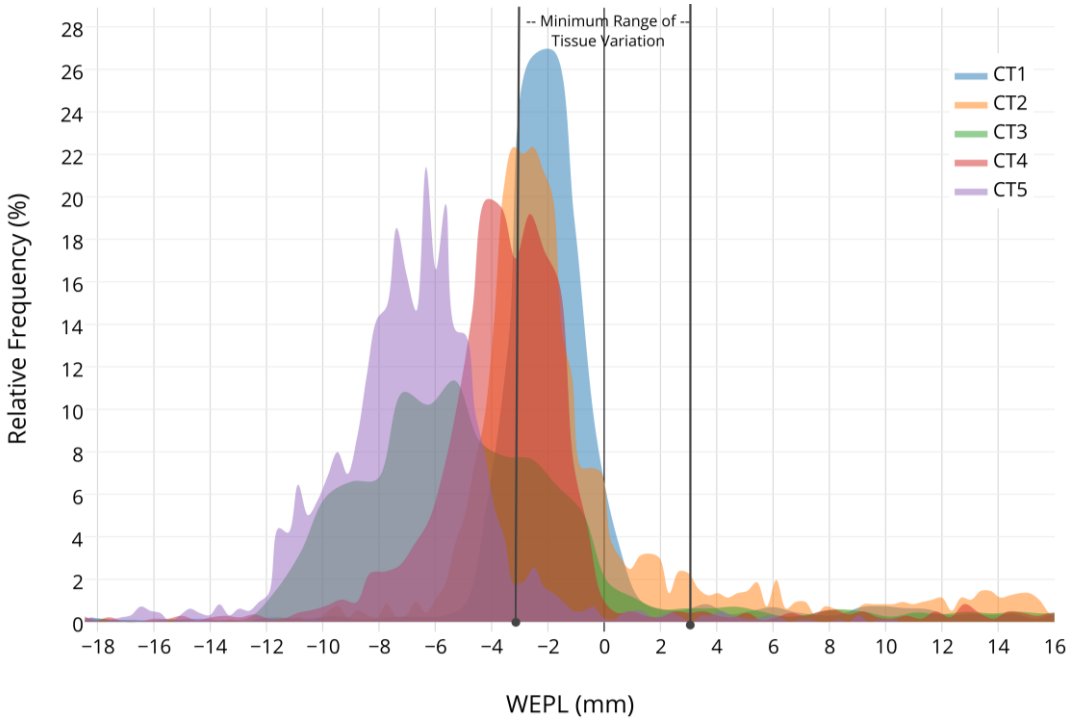

Figure 5.13: Histogram of accWEPL difference map for the Field 2; all the CTs of patient J.

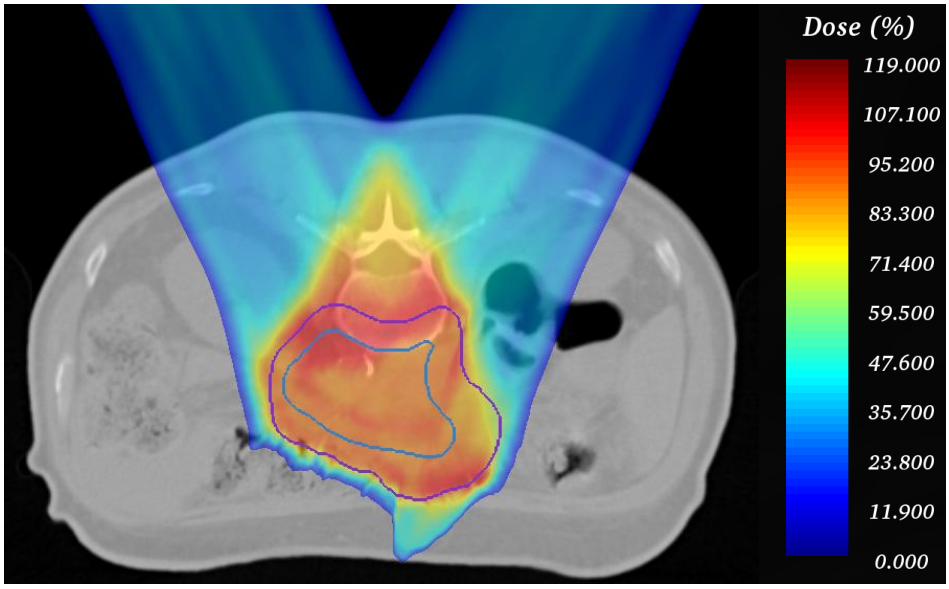

Figure 5.14: Dose distribution of patient J weekly-CT1. This demonstrates how bowel movement effects the dose distribution. (blue = CTV and purple = PTV)

It has been found that the major cause of very low PV_{norm}, i.e. strong WEPL variations, is the bowel movement for this patient as shown in figure 5.15. This situation effected weekly-CT3 and CT5 the most in terms of PV_{norm} however it was analyzed that the patient had extreme bowel changes along all the weekly-CTs. With this same effect on weekly-CT1 the PV_{norm} was very high and the reason for having high or low PV_{norm} is not only the amount of bowel movement but also how much area of a difference map is filled with lower variations; due to internal organ movement, setup and positioning error; which actually depicts the overall variations experienced in specific treatment field direction. As one can observe in figure 5.15 (a) there are a lot of points with different colors and (b) have most of the area in black meaning points within our range of ±3mm, this same explanation implies to figure 5.12 and 5.13.

Regarding high variation of $V95\%_{PTV}$ in weekly-CT1, was due to the dose limiting OARs invading PTV which result in compromised coverage of the target as shown in figure 5.14. Since both the treatment field weight was almost equal contributed in decreased dose conformity.

All in All, patient J partially satisfies the defined criteria for all the weekly-CTs where weekly-CT2 represents a case which stays above the tolerance level. Weekly-CT1 and CT4 will fall in the tolerance level because the PV_{norm} was almost 70% or lower. Although weekly-CT3 and CT5 stayed in action level, with PV_{norm} lower than 56% representing more than 3% variation in $V95\%_{PTV}$ and gamma passing rate as low as 96.5%.

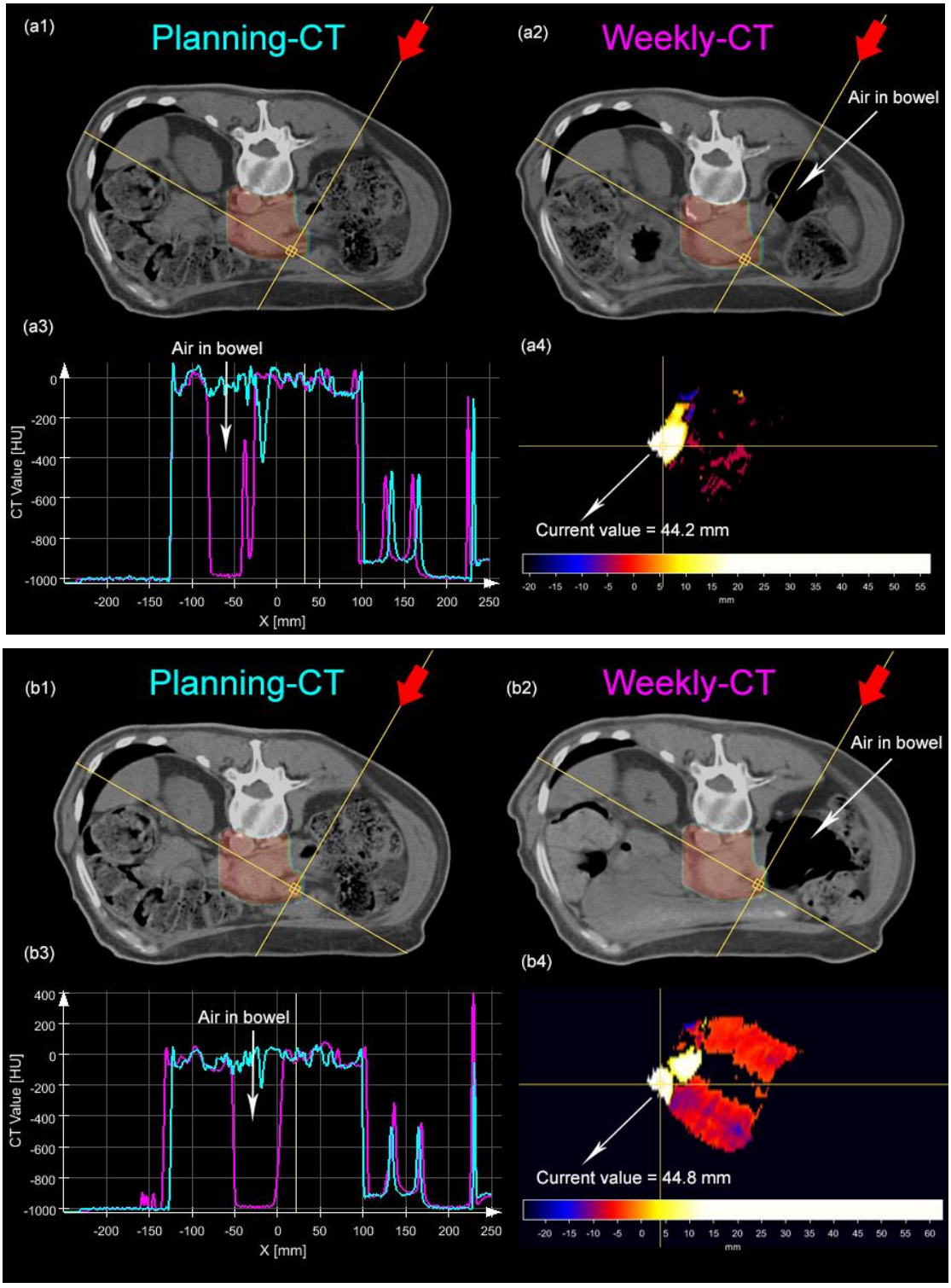

Figure 5.15: Point analysis for Patient J (a) For Weekly-CT1, field 2, (b) For weekly-CT3, field 2. The bowel changes effect from planning-CT and weekly-CT can be observed in CT value (HU) and also in accWEPL difference map. In (a4, b4) the current value is the accWEPL value for the specific beam indicated by red arrow in (a1, a2, b1, b2). The important thing is the area of the difference map in (a4) filled with variations, most of the area is black which represents points within ±3mm. (Note: Apparently scan images are deformed because of the couch angle used and this is how software will look through that beam; the software doesn't apply this deformation while calculating accWEPL)

2 - Patient F

The dose distribution of patient F has been shown in figure 5.16, see table 3.1 for further details about field configuration, dose per fraction and number of weekly-CTs. This patient is one of those patients who had fluctuating variation of $V95\%_{CTV}$ for all the weekly-CTs which was up to 2% as shown in figure 3.10. Although $V95\%_{PTV}$ variation was up to 7% for first weekly-CT represented as a worst case and within 3% for the remaining weekly-CTs as shown in figure 3.3. The DVH of CTV and PTV in figure 5.17 shows the variation from planning-CT to weekly-CTs. The $V95\%_{CTV}$ (where 95% dose is 1.9GyE) for planning-CT was 98% and decreased to 95% for weekly-CT1. The $V95\%_{PTV}$ for planning-CT was almost 90% and decreased up to 83% for the weekly-CT1 as well.

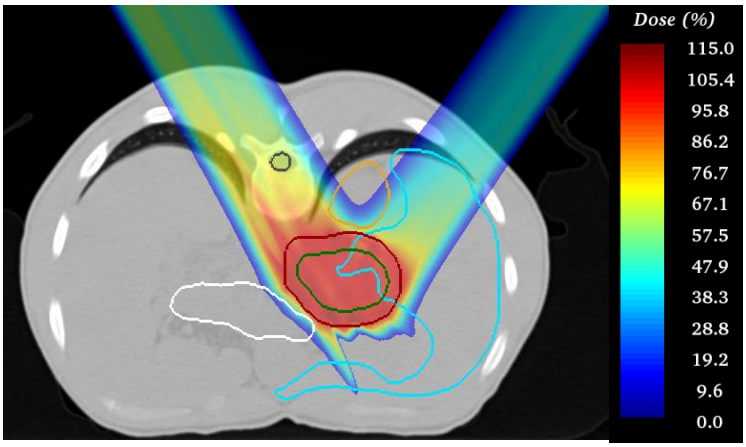

Figure 5.16: Dose distribution of a planning-CT for Patient F. (Contoured OARs and target volumes: grey = spinal cord, mustard = right kidney, white = bowel, aqua = liver, green = CTV, red = PTV)

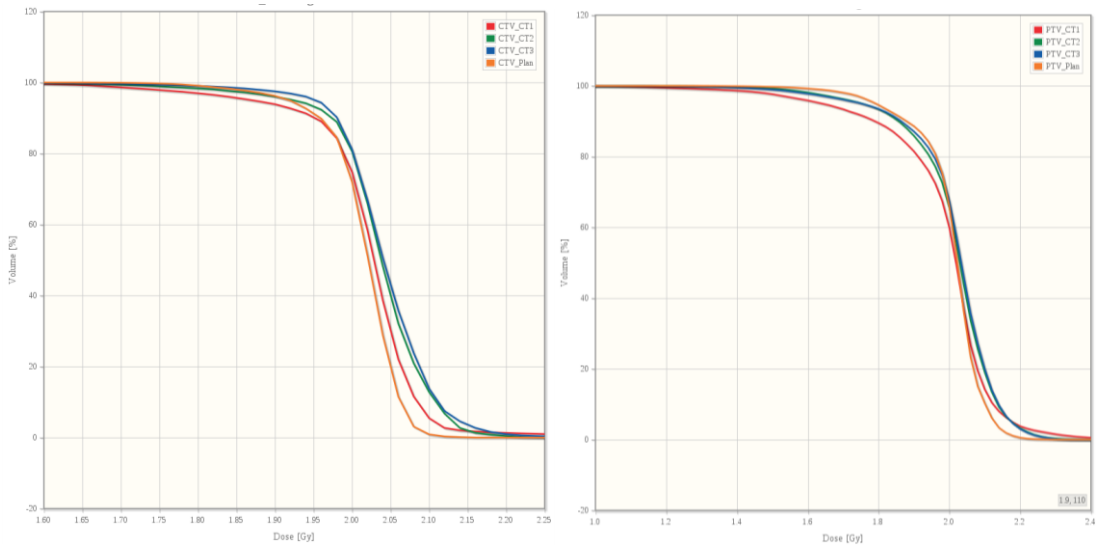

Figure 5.17: DVH of CTV (left side) and PTV (right side) for patient F including planning-CT and 3 weekly-CTs; where 95% dose is 1.9GyE

This patient represents lowest and consistent value for PV_{norm} along the weekly-CTs, see figure 5.18. The weekly-CT1 represents more than 7% variation in PTV V95% and gamma passing rate slightly lower than 96.5%. In weekly-CT2, gamma passing rate was higher but there was more than 2% variation in $V95\%_{PTV}$. On the contrary weekly-CT3 even with low PV_{norm} does not follow any of the defined criteria which make it a special case to root analyze the possible reasons.

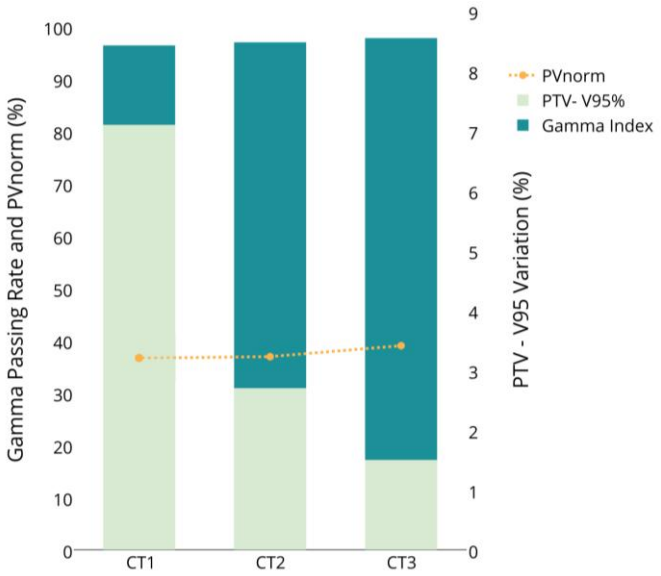

Figure 5.18: Bar graph for Patient F. All the weekly-CTs represent lower PV_{norm} correspond and only weekly-CT1 with high variation in V95% PTV, gamma passing rate was high for all weekly-CTs

Figure 5.19: The registration images of patient F for all the weekly-CTs. The worst case was weekly-CT1 and the remaining were better than weekly-CT1 (red= planning-CT, aqua= weekly-CT)

After the detailed analysis it turned out that this patient had a surgery after having a planning-CT which resulted in worst case for the registration (it should be noted that these results are from image registration, does not mean these errors were the same during the actual treatment). As shown in figure 5.19, the image registration was worst for the weekly-CT1 and gradually got slightly better for weekly-CT2 and

CT3. For this patient, surgery was not the only problem but extreme positioning errors affected the registration results simultaneously.

As described above, the reason for having low quality image registration, similar applies to WEPL maps which require image registration of planning and weekly-CTs. It was observed from figure 5.20 the peaks representing majority of the variations laid outside the defined minimum range of tissue variation ±3 mm for field 1 of all the weekly-CTs. On the other hand figure 5.21 showed peaks of variations within the range of ±3 mm for field 2 thus the combine effect from both the field resulted in low PV_{norm}.

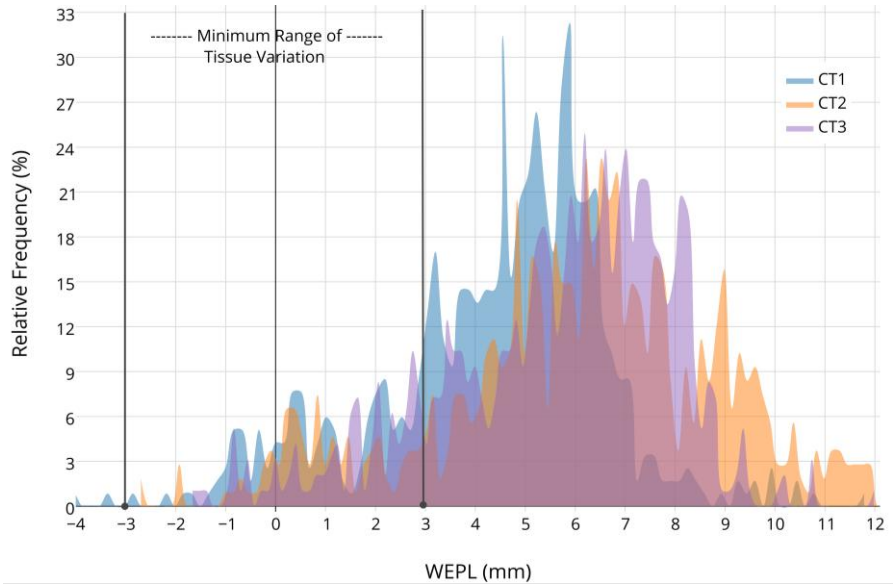

Figure 5.20: Histogram of accWEPL difference map for field 1; all weekly-CT's of Patient F

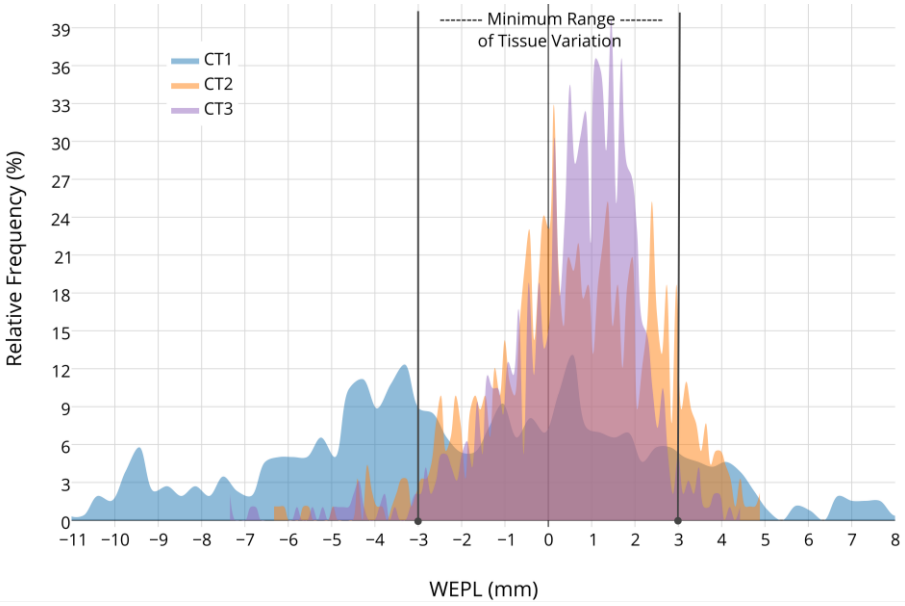

Figure 5.21: Histogram of accWEPL difference map for field 2; all weekly-CTs of Patient F

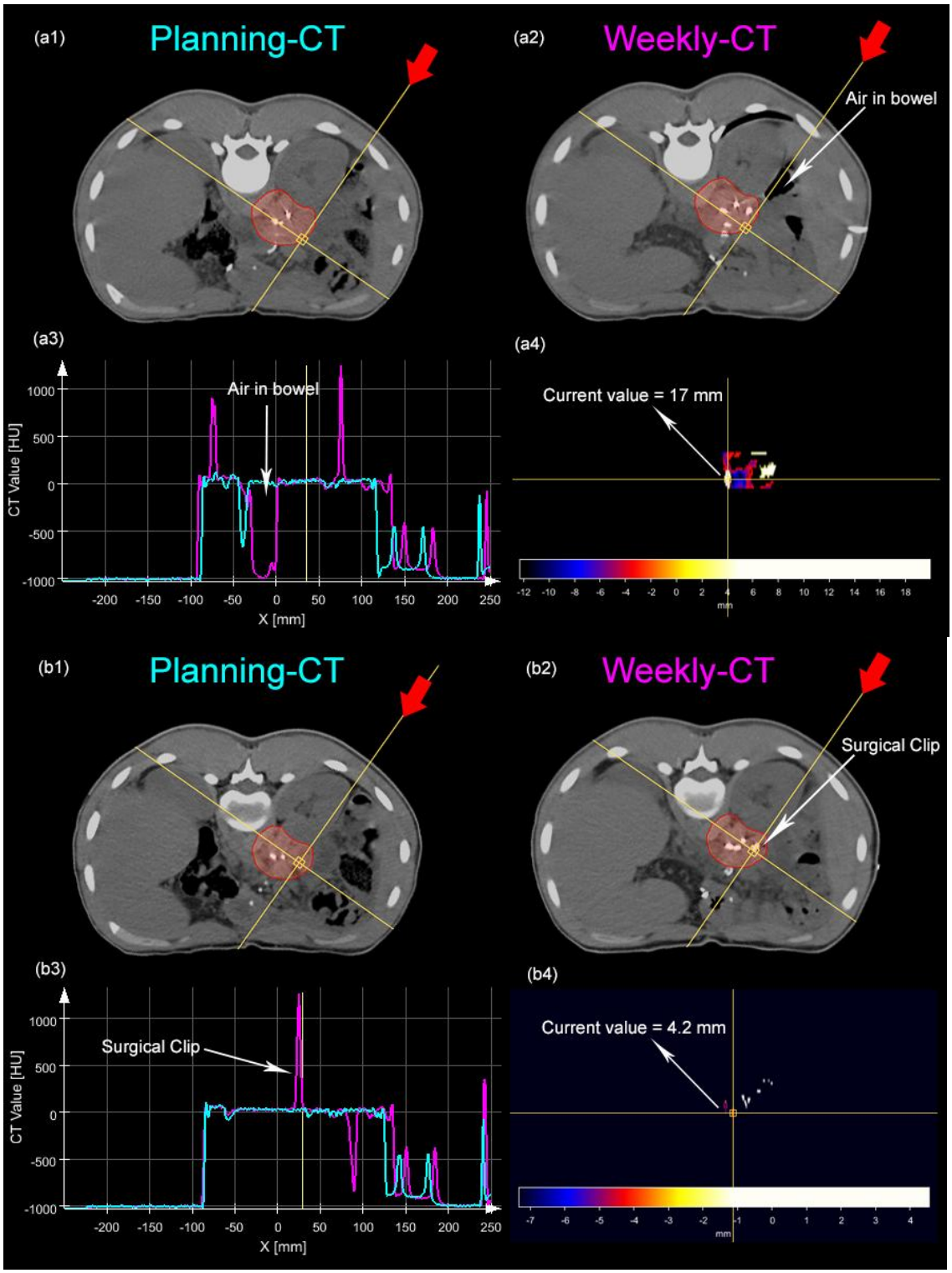

Figure 5.22: Point analysis for Patient F. (a) For Weekly-CT1, field 2. (b) For weekly-CT3, field 2. The bowel changes effect from planning-CT (a1) and weekly-CT (a2) can be observed in (a3) CT value (HU) and also in (a4) accWEPL difference map. The current value is the accWEPL value for that specific beam indicated by red arrow. The movement of surgical clip in planning-CT (b1) and weekly CT (b2) can be observed and the resulting effect in (b3) CT value (HU) and (b4) accWEPL difference map. Again one can compare the area of the difference map filled with variations, for weekly-CT1 a lot of points with variations but in weekly-CT3 most of the area is black which represents points within ±3mm.

After point analysis on all the weekly-CTs shown in figure 5.22, it was proven that major density variations were due to positioning error, surgical clip movement and amount of lung in the beam's path. Since this patient had small target volume the aforementioned effects were prominent for this patient although changes in bowel movement were not dominant as seen in previous patient example.

On the whole, weekly-CT1 demonstrated $V95\%_{PTV}$ variation up to 7% and gamma passing rate 96.4% with PV_{norm} lower than 56%, these result were in accordance with the action level criteria. However weekly-CT2 and CT3 represents as those cases which are difficult to decide by relying only on one parameter thus would require further investigation.

5.5 Summary

In this chapter, a strong correlation was found among PTV, gamma passing rate and WEPL variation. By analysis of this correlation the criteria was defined for PV_{norm} as tolerance and action level which was justified by the patient examples from this study.

Chapter 6

Discussion and Conclusion

6.1 Discussion

From the last few years charged particle therapy has become a popular treatment option for the pancreatic cancer. Many radiation oncologists opt for it to deliver an effective and precise dose to pancreatic tumor surrounded by dose limiting critical structures such as bowel, liver, kidney and spinal cord. There are several studies which explain the improved results of charged particle therapy over photons IMRT. The special concern is usually given to reduce the dose to OARs that is certainly achieved by charged particle therapy due to their finite range. In one of the comparative studies Zurlo [43] discussed about proton therapy over photon therapy for pancreatic cancer, authors examined the treatment dosimetry plans and found that proton therapy has the potential to achieve superior absorbed dose distributions compared with photon therapy.

Further attention was given to optimize the treatment plans by achieving suitable beam geometry. As Dreher et al [44] studied different beam geometries for the treatment of pancreatic cancer using raster-scanning technique and suggested that 3-field configuration have the best dose distribution, single treatment field is robust however 2 oblique posterior fields is most favorable. The result from this study has been implemented in HIT facility for the treatment of pancreatic cancer that is why in this work the majority of the patients have 2 oblique posterior fields. An additional study by Batista [45] was conducted by taking into account the inter and intra-fractional motion effects on the target coverage using scanned carbon ion beams and suggested that 2 oblique posterior treatment fields is a robust beam geometry to minimize the dose degradation due to organ motion for the treatment of pancreatic cancer.

Since internal organ motion could largely affect the range of charged particles resulting in high dose to OARs, many mitigation techniques have already been considered such as respiratory gating and abdominal compression. Although abdominal compression has been implemented in HIT facility for liver tumors, for pancreatic patients due to the use of posterior beams and in order to avoid radiation beam through the couch, the patients are positioned prone which makes impossible

the use of abdominal compression. Further improvement was investigated by Richter [46] and found that by increasing the treatment beam spot size the dose heterogeneity caused by motion could be reduced.

Adaptive therapy is considered a promising option to overcome the inter-fractional motion. There are several studies on head and neck tumors which emphasis on the need of adaptive particle therapy for example Thomson et al [47] discussed the impact of organ motion on oropharynx cancer. The author suggested that protons are much sensitive to inter-fractional anatomic changes which could result in clinically significant increased delivered doses to several OARs and emphasized on adaptation of those changes during the course of treatment. Although, Chen et al [48] suggested an adaptive strategy by expanding the dosimetry plan library for a specific patient and implementing it depending on the best anatomical match. Authors created offline plans on daily CT, starting from first fraction and used those plans for subsequent fractions which have similar anatomic changes. This strategy seems difficult to implement in daily clinical routine because of the time consumption when creating new treatment plans.

As researchers are consistently proposing new ways of adaptive therapy, similarly, the rationale of this thesis was also to develop the criteria which could help in treatment plan adaptation by simplest means and clinically applicable to the HIT clinical routine. This work investigated motion effect on the WEPL and its correlation to the variation of dosimetric parameters. The results were similar to the study from Matney [49] where author found no significant correlation of tumor centroid motion with change in dose, in section 3.8 the variation of $V95\%_{CTV}$ has been discussed and found that CTV coverage remained uniformed for most of the patients and this was verified by correlating it to PV_{norm} which showed weak correlation. Further Matney outlines the strong correlation of WEPL with change in dose and gamma passing rate which is similar to the presented results in section 5.1.2 and 5.1.3.

From the results of WEPL variation, it was found that surgical clip present within the CTV have been one of the cause of variation, for all the patient of this study. Its movement was regulated by the tumor motion itself resulting in different position on every fraction. Van der Horst performed a study [50] to quantify the inter-fractional movement of surgical clip in pancreatic tumors; investigation revealed that there is 10 mm variation on a daily basis. This result explains the reason for having WEPL variation in CTV.

Kumagai et al [51] investigated carbon ion beam dose variation due to bowel gas movement in pancreatic radiotherapy, however it was done for intra-fractional motion. The results from this study suggested that there was variation in target conformity (approx 3% for CTV) resulting in dose degradation due to over or undershoot of the beam, also excessive dosage found to the OARs. Aforementioned effects were also the result of the presented study where large variations were observed for $V95\%_{PTV}$ (mean variation 2.2%) and $V95\%_{CTV}$ (mean variation 1.4%) this was justified by corresponding WEPL variations, as explained in section 5.2.1 with an example.

In section 5.2.1, patient F example was explained and it was found that WEPL variation is high for the weekly-CTs but $V95\%_{PTV}$ of two weekly-CT represented slight variation; one of the suggested reasons for such result was the size of the tumor. That patient was comparatively younger than other patients included in this study thus the size of the CTV was also relatively small. Moreover patient had a surgery as well before the treatment. This effect is explained by Zurlo [43] in a study where large volumes were investigated for the treatment of pancreatic tumor irradiated with protons. One of the results found by the author was that for small tumors or postoperative patient target dose conformity was superior to those with unresectable or large tumors, however, doses to OARs were still close to the maximum limit tolerance defined.

In the presented work, it was assumed that patients were precisely immobilized but the similar patient example which was explained above emphasizes on further improvement regarding patient positioning and setup errors. For this case it was found that large variation in WEPL was primarily due to extreme error in patient positioning however these are possible errors came up after the image registration. Despite the fact that prone position is the requirement of robust beam configuration explained earlier, it is suggested that body mask would be a considerable option for these setups.

From this work it was found that using WEPL for the assessment of density variation on a daily basis is less time consuming which could hardly take 5 minutes for calculation which is suitable time duration for making a decision in a practical scenario. This was also suggested by Matney et al [49] where they found very less computational time for the calculation of WEPL.

6.2 Conclusion

This thesis investigated the impact of inter-fractional motion on dosimetric parameters that resulted in major density variation in particle therapy. Similar investigation was performed using WEPL as a clinical metric to quantify the resulting effect of inter-fractional motion. The study revealed strong correlation of variation in dose distribution and WEPL due to density variations. The evaluation of WEPL has led in this work to develop the criteria for WEPL which could be used as a tool for the physicians to predict the necessity of treatment plan adaptation. Fast calculation of WEPL with less hassle is a proven advantage found through this work. However it is a small retrospective study with limited statistical power but encourages further efforts with higher patient numbers to refine the suggested criteria. Since this thesis only considers inter-fractional motion, the work can be improved by taking into account of intra-fractional motion.

Appendix

A.1 Dosimetric and WEPL Evaluation Parameters

Table A.1 (a): Evaluation of dose distribution for all the patients included in this thesis. This table includes $V95\%_{PTV}$ variation, maximum dose of PTV, Dmin PTV and Dmean PTV.

Patient	CT	$V95\%_{PTV}$ Variation (%)	Max. Dose of PTV (GyE)	PTV D_{min} (GyE)	PTV D_{mean} (GyE)
A	Plan	-	2.05	0.48	1.76
	1	0.31	2.16	0.32	1.76
	2	1.83	2.13	0.14	1.75
	3	0.85	2.24	0.38	1.76
	4	1.83	2.12	0.39	1.76
	5	1.50	2.07	0.10	1.75
	Mean	1.26	2.13	0.30	1.76
	Std dev	0.59	0.07	0.15	0.01
B	Plan	-	2.10	0.27	1.78
	1	4.75	2.10	0.01	1.73
	2	4.33	2.08	0.01	1.73
	3	6.52	2.09	0.02	1.70
	Mean	5.20	2.09	0.08	1.73
	Std dev	0.94	0.01	0.13	0.03
C	Plan	-	2.24	0.07	1.67
	1	0.02	2.28	0.11	1.66
	2	0.07	2.26	0.11	1.67
	3	0.00	2.28	0.21	1.67
	Mean	0.03	2.27	0.12	1.67
	Std dev	0.02	0.02	0.06	0.00
D	Plan	-	2.03	0.43	1.76
	1	0.37	2.11	0.59	1.76
	2	1.25	2.10	0.70	1.75
	3	1.36	2.11	0.63	1.75
	Mean	0.99	2.09	0.59	1.75
	Std dev	0.44	0.04	0.12	0.01
E	Plan	-	2.11	0.25	1.76
	1	4.78	2.15	0.16	1.75
	2	2.29	2.17	0.40	1.76
	3	1.65	2.19	0.17	1.75
	Mean	2.90	2.15	0.25	1.75
	Std dev	1.35	0.03	0.11	0.01

Continuation of table A.1 (a)

Patient	CT	V95%PTV Variation (%)	Max. Dose of PTV (GyE)	PTV Dmin (GyE)	PTV Dmean (GyE)
F	Plan	-	2.30	1.22	2.00
	1	7.13	2.63	0.94	1.98
	2	2.79	2.40	1.20	2.00
	3	1.51	2.34	1.10	2.02
	Mean	3.81	2.42	1.12	2.00
	Std dev	2.40	0.15	0.13	0.02
G	Plan	-	2.63	0.97	1.78
	1	0.46	2.63	0.81	1.78
	2	0.26	2.17	0.33	1.76
	3	0.36	2.64	0.84	1.77
	Mean	0.36	2.52	0.73	1.77
	Std dev	0.08	0.23	0.28	0.01
H	Plan	-	2.19	0.91	1.78
	1	0.57	2.19	0.79	1.78
	2	2.52	2.23	0.41	1.78
	3	2.89	2.24	0.90	1.78
	4	1.24	2.24	1.29	1.78
	Mean	1.80	2.22	0.86	1.78
	Std dev	0.92	0.03	0.32	0.00
I	Plan	-	4.31	2.40	3.80
	1	1.75	4.33	2.28	3.79
	Mean	1.75	4.32	2.34	3.80
	Std dev	0.00	0.01	0.09	0.01
J	Plan	-	2.10	0.94	1.74
	1	2.65	2.13	0.52	1.73
	2	0.10	2.15	0.57	1.72
	3	2.79	2.22	0.18	1.68
	4	1.17	2.15	0.19	1.71
	5	4.88	2.21	0.04	1.67
	Mean	2.31	2.16	0.41	1.71
	Std dev	1.62	0.05	0.33	0.03
K	Plan	-	2.12	0.65	1.79
	1	2.43	2.17	0.13	1.78
	2	3.40	2.35	0.15	1.79
	3	0.85	2.32	0.40	1.80
	4	2.55	2.35	0.12	1.79
	5	3.49	2.27	0.29	1.80
	6	3.70	2.34	0.81	1.78
	Mean	2.73	2.28	0.36	1.79
	Std dev	0.96	0.09	0.27	0.01

Table A.1 (b): Evaluation of dose distribution and WEPL assessment for all the patients included in this thesis. This table includes $V95\%_{CTV}$ variation, gamma passing rate and PV_{norm} in the WEPL distal and proximal analysis.

Patient	CT	$V95\%_{CTV}$ Variation (%)	Gamma Passing Rate (%)	Distal PV_{norm} (%)	Proximal PV_{norm} (%)
A	Plan	-	-	-	-
	1	1.68	98.6	72.7	71
	2	0.61	97.5	75.5	77
	3	1.75	98.5	79.1	82.5
	4	1.95	98.2	72.2	75.7
	5	0.77	98.7	60.2	59.5
	Mean	1.35	98.2	71.9	73.1
	Std dev	0.55	0.48	6.3	7.7
B	Plan	-	-	-	-
	1	3.63	96.7	69.3	77
	2	2.71	96.8	51.6	52
	3	4.05	96.5	50.3	50.7
	Mean	3.46	96.6	57	59.9
	Std dev	0.55	0.15	8.6	12.1
C	Plan	-	-	-	-
	1	0.36	99.3	81.3	90.1
	2	0.92	98.9	73.7	80.4
	3	0.89	98.6	85.7	94.3
	Mean	0.72	98.9	80.2	88.2
	Std dev	0.25	0.35	4.9	5.8
D	Plan	-	-	-	-
	1	0	99.7	98.1	98.1
	2	0.28	98.8	88.9	89.3
	3	0.47	99.2	79.2	80.3
	Mean	0.25	99.2	88.7	89.2
	Std dev	0.19	0.45	7.7	7.2
E	Plan	-	-	-	-
	1	1.27	97.5	76.9	74.7
	2	1.1	97.8	66.5	67.4
	3	0.82	98.7	81.7	82.8
	Mean	1.06	98	75	74.9
	Std dev	0.18	0.62	6.3	6.2

Continuation of table A.1 (b)

Patient	CT	V95%CTV Variation (%)	Gamma Passing Rate (%)	Distal PVnorm (%)	Proximal PVnorm (%)
F	Plan	-	-	-	-
	1	2.35	96.4	36.6	30.8
	2	0.18	97	36.9	36.3
	3	1.27	97.8	39	38.1
	Mean	1.26	97	36.6	35
	Std dev	0.88	0.7	1	3.1
G	Plan	-	-	-	-
	1	0.14	99.5	98.7	98.9
	2	0.79	98.8	74.7	74.7
	3	0.29	99.2	83.1	83
	Mean	0.4	99	85.5	85.5
	Std dev	0.27	0.35	9.9	10
H	Plan	-	-	-	-
	1	0.03	97.6	70.3	71.5
	2	2.27	97.9	67.6	74.1
	3	2.31	97.5	69.9	70.5
	4	0.36	95.8	72.1	73.4
	Mean	1.24	97	69.9	72.3
	Std dev	1	0.94	1.6	1.4
I	Plan	-	-	-	-
	1	0.12	96.7	54.4	59
	Mean	0.12	96.7	54.5	59
	Std dev	0	0	0	0
J	Plan	-	-	-	-
	1	1.7	97.7	71.9	76
	2	0.2	96.7	71.8	72.6
	3	1	92.7	35.1	35.7
	4	0.3	94.7	65.7	69.5
	5	0.5	91.3	23	23.6
	Mean	0.74	94.6	53.5	55.4
	Std dev	0.55	2.6	20.4	21.5
K	Plan	-	-	-	-
	1	13.6	96.4	71.5	45.8
	2	8.1	96	65.1	67.2
	3	4.8	98.4	74.4	73.1
	4	9.7	96.6	73.7	75.6
	5	4.9	97.2	55.9	51.1
	6	0.4	97.9	59.6	62
	Mean	6.9	97	66.1	62.5
	Std dev	4.1	0.92	7	11.9

A.2 OAR analysis

Table A. 2: Dose evaluation of OARs. This table includes bowel V20%, bowel V80%, kidneys V40% and D_{max} spinal cord.

Patient	CT	Bowel		Kidney V40 (%)		Spinal Cord Dmax (GyE)
		V20 (%)	V80 (%)	Right	Left	
A	Plan	19.90	9.10	46.80	41.60	1.45
	1	21.50	12.70	35.80	31.70	1.49
	2	23.60	14.40	36.80	36.60	1.47
	3	24.40	14.70	31.30	39.80	1.47
	4	22.50	13.40	36.40	37.90	1.47
	5	20.10	12.40	37.20	36.30	1.45
	Mean	22.00	12.78	37.38	37.32	1.47
B	Plan	12.90	8.90	11.60	9.10	1.47
	1	16.40	10.50	15.40	11.00	1.50
	2	16.90	11.90	17.20	11.30	1.45
	3	24.00	16.90	15.40	11.40	1.47
	Mean	17.55	12.05	14.90	10.70	1.47
C	Plan	23.80	10.00	13.00	19.30	1.60
	1	14.40	6.00	15.30	18.40	1.60
	2	14.40	6.30	14.00	18.70	1.69
	3	17.70	7.70	13.00	18.50	1.65
	Mean	17.58	7.50	13.83	18.73	1.64
D	Plan	12.60	5.25	17.70	17.70	1.36
	1	3.00	1.17	16.10	20.10	1.33
	2	10.00	5.50	22.50	16.30	1.36
	3	11.80	7.50	10.80	15.20	1.35
	Mean	9.35	4.86	16.78	17.33	1.35
E	Plan	18.20	8.25	18.30	17.90	1.51
	1	15.20	6.60	21.40	21.90	1.47
	2	21.00	11.60	14.50	23.70	1.49
	3	20.80	12.00	15.60	27.40	1.49
	Mean	18.80	9.61	17.45	22.73	1.49

Continuation of table A.2

Patient	CT	Bowel		Kidney V40 (%)		Spinal Cord Dmax (GyE)
		V20 (%)	V80 (%)	Right	Left	
F	Plan	9.30	1.67	17.60	4.10	1.68
	1	10.40	1.90	18.60	3.98	1.64
	2	9.80	1.80	17.70	4.00	1.66
	3	10.00	1.50	17.70	4.00	1.68
	Mean	9.88	1.72	17.90	4.02	1.67
G	Plan	11.90	3.43	31.00	28.60	1.56
	1	6.80	1.14	29.70	36.00	1.56
	2	9.70	2.42	24.00	35.30	1.58
	3	12.00	4.80	30.20	40.70	1.54
	Mean	10.10	2.95	28.73	35.15	1.56
H	Plan	11.10	3.50	12.20	17.30	1.38
	1	10.50	3.00	14.10	19.60	1.40
	2	11.10	3.50	11.00	14.40	1.38
	3	13.10	4.90	12.70	18.30	1.40
	4	14.00	5.60	13.20	15.50	1.40
	Mean	11.96	4.10	12.64	17.02	1.39
I	Plan	12.30	4.79	11.10	0.00	2.70
	1	12.50	4.88	7.95	0.00	2.70
	Mean	12.40	4.84	9.53	0.00	2.70
J	Plan	24.30	11.30	13.50	36.00	1.60
	1	23.60	9.80	13.40	36.00	1.60
	2	23.00	9.70	14.00	38.00	1.60
	3	22.70	8.00	14.20	40.00	1.60
	4	22.40	8.50	13.60	39.00	1.60
	5	21.60	7.30	14.50	40.00	1.60
	Mean	22.93	9.10	13.87	38.17	1.60
K	Plan	23.00	13.70	22.50	20.40	1.36
	1	20.30	11.80	22.80	21.40	1.36
	2	20.70	12.60	22.20	21.80	1.36
	3	21.80	12.90	22.60	20.20	1.36
	4	20.40	12.30	22.50	21.40	1.38
	5	21.20	13.00	22.30	21.90	1.36
	6	22.70	13.40	22.60	20.20	1.33
	Mean	21.44	12.81	22.50	21.04	1.36

A.3 Absorbed Dose Distributions

Figure A. 3: The dose distribution for all the patients included in this study. (Contoured OARs and target volumes: grey = spinal cord, lime = left kidney, mustard = right kidney, white = bowel, green = CTV, red = PTV)

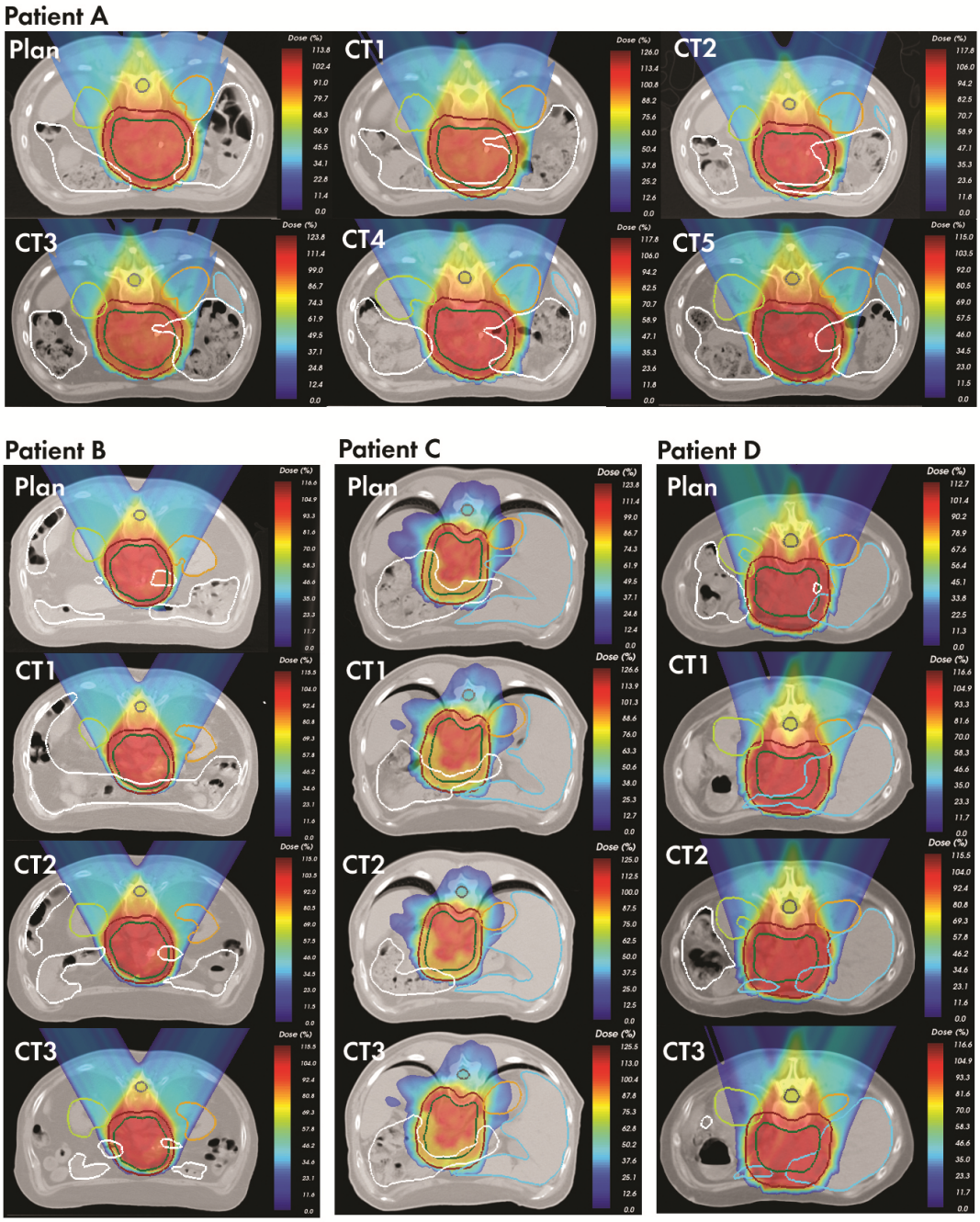

Continuation of figure A.3

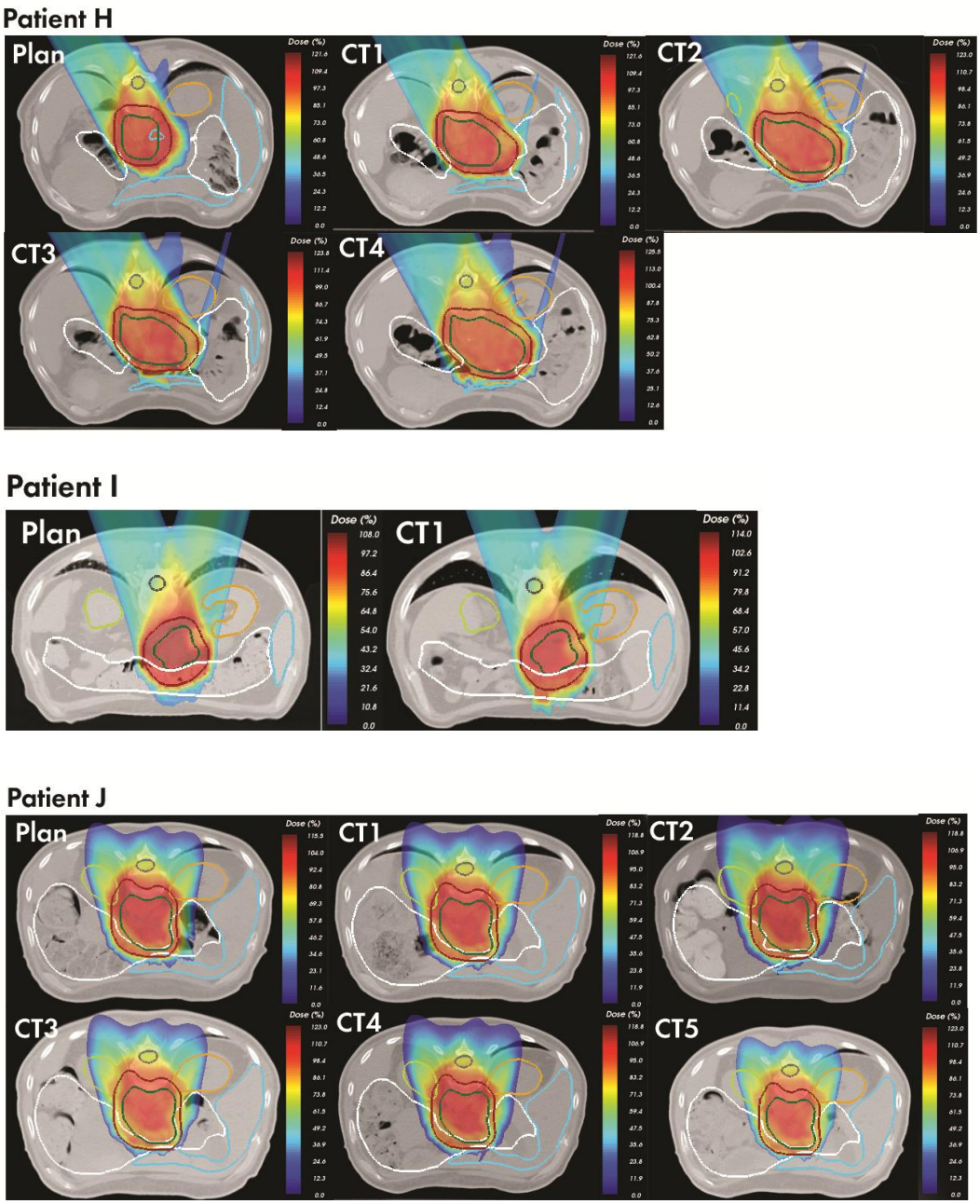

Continuation of figure A.3

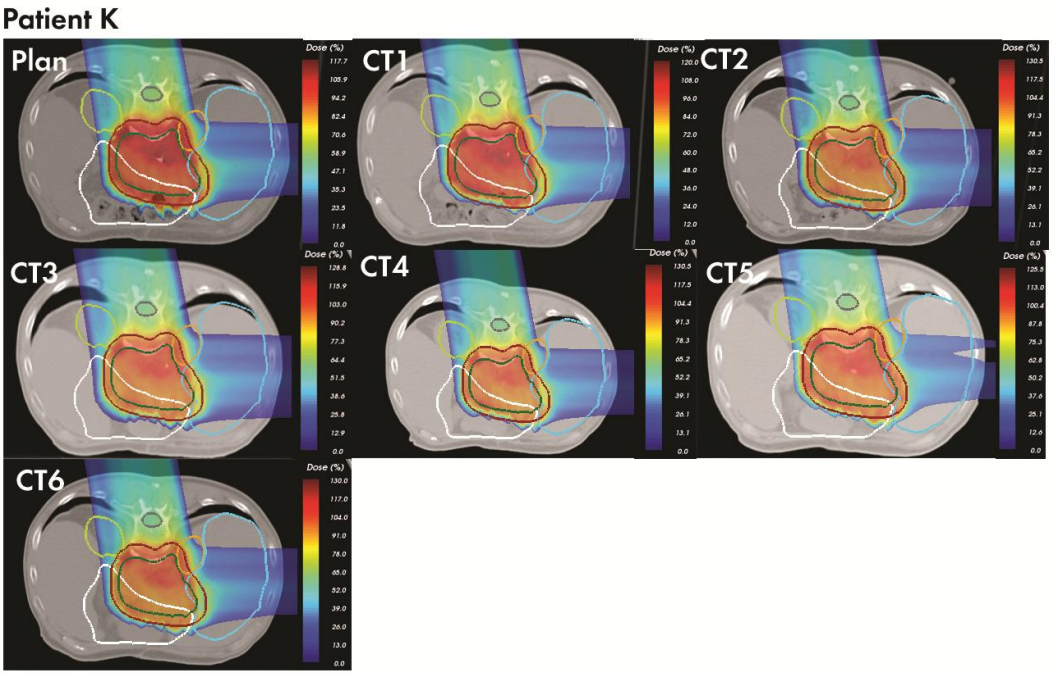

Bibliography

[1] Ferlay J, Soerjomataram I, Ervik M, Dikshit R, Eser S, Mathers C, Rebelo M, Parkin DM, Forman D, Bray, F. GLOBOCAN 2012 v1.1, Cancer Incidence and Mortality Worldwide: IARC Cancer Base No. 11 [Internet]. Lyon, France: International Agency for Research on Cancer; 2014. Available from: http://globocan.iarc.fr, accessed on 16/01/2015

[2] Raimondi, Sara, Patrick Maisonneuve, and Albert B. Lowenfels. "Epidemiology of pancreatic cancer: an overview." Nature Reviews Gastroenterology and Hepatology 6.12 (2009): 699-708

[3] H. Ueno, T. Kosuge, Y. Matsuyama et al., “A randomised phase III trial comparing gemcitabine with surgery-only in patients with resected pancreatic cancer: Japanese Study Group of Adjuvant Therapy for Pancreatic Cancer,” British Journal of Cancer, vol. 101, no. 6, pp. 908–915, 2009.

[4] Kozak, Kevin R., et al. "Dosimetric feasibility of hypofractionated proton radiotherapy for neoadjuvant pancreatic cancer treatment." International Journal of Radiation Oncology* Biology* Physics 68.5 (2007): 1557-1566.

[5] Nichols, R. Charles. "Particle therapy for pancreatic cancer." Translational Cancer Research 4.6 (2015): 634-640.

[6] Hsiung-Stripp, Diana C., et al. "Comparative treatment planning between proton and X-ray therapy in pancreatic cancer." Medical Dosimetry 26.3 (2001): 255-259.

[7] Bouchard, Myriam, et al. "Dose escalation with proton or photon radiation treatment for pancreatic cancer." Radiotherapy and Oncology 92.2 (2009): 238-243.

[8] Ding, Xuanfeng, et al. "A comprehensive dosimetric study of pancreatic cancer treatment using three-dimensional conformal radiation therapy (3DCRT), intensity-modulated radiation therapy (IMRT), volumetric-modulated radiation therapy (VMAT), and passive-scattering and modulated-scanning proton therapy (PT)." Medical Dosimetry 39.2 (2014): 139-145.

[9] Yamada S, Shinoto M, Imada H, Yasuda S, Kamada T, Tsujii H: Carbon ion radiotherapy for patients with gastrointestinal cancer. PTCOG 49. 2010, Chiba, Japan: Ref Type: Generic

[10] Wilson, Robert R. "Radiological use of fast protons." Radiology 47.5 (1946): 487-491.

[11] Tobias, C. A., et al. "Pituitary irradiation with high-energy proton beams a preliminary report." Cancer Research 18.2 (1958): 121-134.

[12] Slater, James M., et al. "The proton treatment center at Loma Linda University Medical Center: rationale for and description of its development."International Journal of Radiation Oncology* Biology* Physics 22.2 (1992): 383-389

[13] Hirao, Y., et al. "Heavy ion synchrotron for medical use—HIMAC project at NIRS-Japan—." Nuclear Physics A 538 (1992): 541-550

[14] PTCOG 2016. www.ptcog.ch

[15] Levin, W. P., et al. "Proton beam therapy." British journal of Cancer 93.8 (2005): 849-854.

[16] Giap, Huan, and Bosco Giap. "Historical perspective and evolution of charged particle beam therapy." Translational Cancer Research 1.3 (2012): 127-136

[17] Quantities, I. C. R. U. "Units in Radiation Protection Dosimetry. ICRU Report 51." (1993)

[18] Linz, Ute, ed. Ion Beam Therapy: Fundamentals, Technology, Clinical Applications. Springer Science & Business Media, 2011

[19] Schardt, Dieter, Thilo Elsässer, and Daniela Schulz-Ertner. "Heavy-ion tumor therapy: Physical and radiobiological benefits." Reviews of modern physics82.1 (2010): 383

[20] Weber, Uli, and Gerhard Kraft. "Comparison of carbon ions versus protons."The Cancer Journal 15.4 (2009): 325-332

[21] Hsiao-Ming Lu, Ph.D., Jay Flanz, Ph.D., Harald Paganetti, Ph.D.”Physics of Particle Beams”. PTCOG 53 Education Session, Shanghai, 2014

[22] Paganetti, Harald, et al. "Relative biological effectiveness (RBE) values for proton beam therapy." International Journal of Radiation Oncology* Biology* Physics 53.2 (2002): 407-421.

[23] Johansson, Jonas. "Comparative treatment planning in radiotherapy and clinical impact of proton relative biological effectiveness." (2006)

[24] Kraft, G., and S. D. Kraft. "Research needed for improving heavy-ion therapy." New Journal of Physics 11.2 (2009): 025001

[25] Elsässer, Thilo, Michael Krämer, and Michael Scholz. "Accuracy of the local effect model for the prediction of biologic effects of carbon ion beams in vitro and in vivo." International Journal of Radiation Oncology* Biology* Physics71.3 (2008): 866-872

[26] Khan, Faiz M., and John P. Gibbons. Khan's the physics of radiation therapy. Lippincott Williams & Wilkins, 2014

[27] Chu, W. T., B. A. Ludewigt, and T. R. Renner. "Instrumentation for treatment of cancer using proton and light-ion beams." Review of Scientific Instruments 64.8 (1993): 2055-2122

[28] Kanai, Tatsuaki, et al. "Three-dimensional beam scanning for proton therapy." Nuclear Instruments and Methods in Physics Research 214.2-3 (1983): 491-496

[29] Haberer, Th, et al. "Magnetic scanning system for heavy ion therapy."Nuclear Instruments and Methods in Physics Research Section A: Accelerators, Spectrometers, Detectors and Associated Equipment 330.1 (1993): 296-305

[30] Prescribing, I. C. R. U. "Recording, and Reporting Proton-Beam Therapy ICRU Report 78." J ICRU 7.2 (2007): 89-91

[31] Krämer, Michael. "Swift ions in radiotherapy–Treatment planning with TRiP98." Nuclear Instruments and Methods in Physics Research Section B: Beam Interactions with Materials and Atoms 267.6 (2009): 989-992

[32] Podgorsak, Ervin B. "Radiation oncology physics." a handbook for teachers and students/EB Podgorsak.–Vienna: International Atomic Energy Agency657 (2005)

[33] Jones, Douglas. "ICRU report 50—prescribing, recording and reporting photon beam therapy." Medical physics 21.6 (1994): 833-834

[34] Krämer, Michael, and Michael Scholz. "Treatment planning for heavy-ion radiotherapy: calculation and optimization of biologically effective dose."Physics in medicine and biology 45.11 (2000): 3319

[35] Galonska, M., et al. "Commissioning of the ion beam gantry at HIT." IPAC 11 (2011): 2874.

[36] Krämer, Michael, and Michael Scholz. "Treatment planning for heavy-ion radiotherapy: calculation and optimization of biologically effective dose."Physics in medicine and biology 45.11 (2000): 3319.

[37] De Ruysscher, Dirk, et al. "Tumour Movement in Proton Therapy: Solutions and Remaining Questions: A Review." Cancers 7.3 (2015): 1143-1153

[38] Lomax, A. J. "Intensity modulated proton therapy and its sensitivity to treatment uncertainties 1: the potential effects of calculational uncertainties." Physics in medicine and biology 53.4 (2008): 1027.

[39] Yeh, B. K., et al. "Adaptive Replanning is Required During Intensity Modulated Proton Therapy For Head-and-Neck Cancers." International Journal of Radiation Oncology* Biology* Physics 84.3 (2012): S56-S57.

[40] Pieper, Steve, et al. "The NA-MIC Kit: ITK, VTK, pipelines, grids and 3D slicer as an open platform for the medical image computing community."Biomedical Imaging: Nano to Macro, 2006. 3rd IEEE International Symposium on. IEEE, 2006

[41] Low, Daniel A., et al. "A technique for the quantitative evaluation of dose distributions." Medical physics 25.5 (1998): 656-661

[42] di Adroterapia Oncologica, Centro Nazionale. "Plastimatch 1.6–Current Capabilities and Future Directions." Image-Guidance and Multimodal Dose Planning in Radiation Therapy: 108

[43] Zurlo, Alfredo, et al. "The role of proton therapy in the treatment of large irradiation volumes: a comparative planning study of pancreatic and biliary tumors." International Journal of Radiation Oncology* Biology* Physics 48.1 (2000): 277-288

[44] Dreher, Constantin, et al. "Optimization of carbon ion and proton treatment plans using the raster-scanning technique for patients with unresectable pancreatic cancer." Radiation Oncology 10.1 (2015): 1

[45] Batista, V., et al. "Inter-and Intra-fractional Motion Robustness for Pancreatic Patients Treated With Scanned Carbon Ion Therapy." International Journal of Radiation Oncology • Biology • Physics 90.1 (2014): S921

[46] Richter, Daniel, et al. "Residual motion mitigation in scanned carbon ion beam therapy of liver tumors using enlarged pencil beam overlap." Radiotherapy and Oncology 113.2 (2014): 290-295

[47] Thomson, David J., et al. "The Impact of Anatomic Change on Pencil Beam Scanning in the Treatment of Oropharynx Cancer." International Journal of Particle Therapy 2.2 (2015): 394-403

[48] Chen, W., A. Gemmel, and E. Rietzel. "SU-E-T-600: A Study on the Adaptive Strategy 'expanding Treatment Plan Library'for Mitigation of Inter-Fractional Organ Motion." Medical Physics 38.6 (2011): 3627-3627

[49] Matney, Jason E., et al. "Perturbation of water-equivalent thickness as a surrogate for respiratory motion in proton therapy." Journal of Applied Clinical Medical Physics 17.2 (2016).

[50] Van der Horst, Astrid, et al. "Interfractional position variation of pancreatic tumors quantified using intratumoral fiducial markers and daily cone beam computed tomography." International Journal of Radiation Oncology* Biology* Physics 87.1 (2013): 202-208

[51] Kumagai, Motoki, et al. "Impact of intrafractional bowel gas movement on carbon ion beam dose distribution in pancreatic radiotherapy." International Journal of Radiation Oncology* Biology* Physics 73.4 (2009): 1276-1281

[52] Scholz, M. and Kraft, G. (1996). Track structure and the calculation of biological effects of heavy charged particles. Adv. Space Res., 18:5–14

[53] Rietzel, Eike, and Christoph Bert. "Respiratory motion management in particle therapy." Medical physics 37.2 (2010): 449-460

[54] Mihailescu, Dan. "Biophysical models in hadrontherapy." Journal of Advanced Research in Physics 3.1 (2012)

[55] Zhu, X. R., et al. "Intensity modulated proton therapy treatment planning using single-field optimization: the impact of monitor unit constraints on plan quality." Medical physics 37.3 (2010): 1210-1219

[56] Jäkel, O., et al. "Relation between carbon ion ranges and x-ray CT numbers." Medical physics 28.4 (2001): 701-703

[57] Schneider, Uwe, et al. "The water equivalence of solid materials used for dosimetry with small proton beams." Medical physics 29.12 (2002): 2946-2951

[58] Schneider, Uwe, Eros Pedroni, and Antony Lomax. "The calibration of CT Hounsfield units for radiotherapy treatment planning." Physics in medicine and biology 41.1 (1996): 111

[59] García-Ramos, José-Enrique, et al., eds. Basic Concepts in Nuclear Physics: Theory, Experiments and Applications: 2015 La Rábida International Scientific Meeting on Nuclear Physics. Vol. 182. Springer, 2016.